STRUCTURAL PHASE TRANSITIONS IN $BaMo_6S_8$: Evidence for an Incommensurate Phase*

J. D. Jorgensen and D. G. Hinks
Materials Science and Technology Division
ARGONNE NATIONAL LABORATORY
Argonne, IL 60439

and

D. M. Hatch and R. M. Putnam
Department of Physics and Astronomy
Brigham Young University
Provo, Utah 84602

ANL/PPRNT--89-95

DE89 008426

January 1986

rt

*Work supported by the U. S. Department of Energy, BES-Materials Sciences, under Contract W-31-109-Eng-38.

STRUCTURAL PHASE TRANSITIONS IN $BaMo_6S_8$:

Evidence for an Incommensurate Phase*

J. D. Jorgensen and D. G. Hinks
Materials Science and Technology Division
ARGONNE NATIONAL LABORATORY
Argonne, IL 60439

and

D. M. Hatch and R. M. Putnam
Department of Physics and Astronomy
Brigham Young University
Provo, Utah 84602

Abstract

The structure of $BaMo_6S_8$ has been studied over the temperature range 19 K to 573 K by time-of-flight neutron powder diffraction. Below 175 K the data can be suitably refined in a triclinic, $P\bar{1}$, cell with volume equal to the rhombohedral, $R\bar{3}$, cell common to most Chevrel-phase structures. At temperatures immediately above 175 K, the rhombohedral, $R\bar{3}$, Bragg peaks are broadened by satellite reflections which appear to be identical to those recently observed at low temperature in $PbMo_6S_8$ and $SnMo_6S_8$. An abrupt change in the sign of the temperature dependence of the hexagonal c axis ($\partial c/\partial T$) signals the transition to an undistorted rhombohedral, $R\bar{3}$, structure at temperatures above about 350 K. An extended Landau theory determines both continuous and discontinuous transitions from $R\bar{3}$ induced by a single order parameter. Analysis of the order parameters inducing commensurate transitions imposes symmetry restrictions on the atomic displacements in the lower symmetry phases. The assumption of an $R\bar{3}$ commensurate phase is not consistent

*Work supported by the U. S. Department of Energy, BES-Materials Sciences, under Contract W-31-109-Eng-38.

with the bond lengths obtained for the distortions to the $P\bar{1}$ (or P1) phase for any of the possible cells preserving order parameters. Thus the phase immediately above 175 K cannot be a commensurate $R\bar{3}$ structure. This is consistent with experimental evidence.

INTRODUCTION

The absence of superconductivity in Chevrel-phase compounds, MMo_6S_8, where the metal ion, M, is Eu^{2+}, Ba^{2+}, Sr^{2+}, or Ca^{2+} was unexplained until the observation by Baillif et al.[1] of a low temperature structural phase transition in $EuMo_6S_8$ and $BaMo_6S_8$ and the subsequent observation by Lackal et al.[2] of what is assumed to be the same transition in $SrMo_6S_8$ and $CaMo_6S_8$. In the first experiment, samples of $EuMo_6S_8$ and $BaMo_6S_8$ were studied by x-ray powder diffraction and found to undergo structural phase transitions at 110 ± 5 K and 175 ± 10 K, respectively. For both systems, the low temperature x-ray patterns were consistent with a triclinic $P\bar{1}$ structure which results from the loss of the threefold axis in the normal rhombohedral, $R\bar{3}$, Chevrel-phase structure. The diffraction line splittings "occurred quasidiscontinuously within a narrow temperature interval" indicating a first order transition. However, the unit cell volume remained practically constant (within 0.1%) through the transition. The loss of superconductivity in the triclinic phases was explained as a lowering of the electron density of states at the Fermi energy when the Mo_6 octahedra distorted from $R\bar{3}$ to $P\bar{1}$ symmetry.[1,3] This explanation was supported by subsequent band structure calculations based on the triclinic $BaMo_6S_8$ structure.[4]

Single crystal x-ray diffraction intensities for $BaMo_6S_8$ were collected at both high and low temperature in order to establish the structural details of the triclinic phase. Unfortunately, the original paper[1] gives only minimal

information about the structure. Some additional structural details, i.e., the dimensions of the Mo_6 octahedra, are quoted in the band structure paper by Nohl et al.[4]

Both $BaMo_6S_8$ and $EuMo_6S_8$ have been shown to superconduct at high pressure with a rather sharp onset pressure which varies with sample preparation and hydrostaticity.[5-9] This sharp onset of superconductivity has been assumed to correspond to a pressure-induced transition from the triclinic, $P\bar{1}$, back to the rhombohedral, $R\bar{3}$ phase. In the case of $EuMo_6S_8$, superconductivity has been reported at pressures above about 7 kbar for sintered samples[6,7] and above 13 kbar for melted samples.[8] In the latter work, it was shown that pressure decreased the transition temperature of the $R\bar{3}$ to $P\bar{1}$ transition and that the pressure-induced onset of superconductivity corresponded to a pressure at which the structural transition was completely suppressed. In the case of $BaMo_6S_8$, pressure-induced superconductivity was initially observed only under nonhydrostatic conditions for pressures above 15 kbar, but not for hydrostatic pressures to 18 kbar.[5] However, more recent results report bulk superconductivity above 19 kbar hydrostatic pressure, confirming that the behavior of $BaMo_6S_8$ and $EuMo_6S_8$ is the same.[9]

The original purpose of the present study was to determine full structural details versus temperature for the $P\bar{1}$ and $R\bar{3}$ phases of $BaMo_6S_8$. However, the experimental data revealed an intermediate phase between the $P\bar{1}$ and $R\bar{3}$ phases of $BaMo_6S_8$ which appears to be identical to the distorted $R\bar{3}$ phase which has been previously reported in $PbMo_6S_8$ and $SnMo_6S_8$.

These experimental observations are consistent with the theoretical treatment of the transition based on an extended Landau theory. A displacive transition from $R\bar{3}$ to $P\bar{1}$ with no change in unit cell does not allow the displacments observed experimentally in the low symmetry phase. However, a

transition from $R\bar{3}$ to $P\bar{1}$ (or P1) is allowed if the two phases are connected by an intermediate, incommensurately-modulated $R\bar{3}$ phase where the modulation eventually locks in to give the $P\bar{1}$ distortion.

EXPERIMENTAL PROCEDURE

A 15g sample of $BaMo_6S_8$ was prepared from a stoichiometric mixture of BaS_x [synthesized from Ba and S], Mo and S in an evacuated, sealed quartz ampoule heated at 1250°C. The sample was fired three times with thorough grinding in an inert atmosphere between each firing. The sample was then checked for impurity phases by x-ray diffraction. Since it is known that synthesis techniques can affect the properties of Chevrel-phase materials, x-ray diffraction was used to determine the temperature of the phase transition for this sample. The x-ray data were collected on a G.E. XRD diffractometer with the sample cooled by a Heli-Tran refrigerator (Air Products and Chemicals, Inc.). The width and peak height of the 223 (hexagonal) Bragg reflection provide a sensitive probe of the transition. These quantities are shown as a function of temperature in Fig. 1. From these data, it is clear than the transition temperature for this sample is 175 K in agreement with the value originally reported by Baillif et al.[1]

For neutron diffraction, the sample was loaded in an 11 mm diameter, 50 mm long sealed vanadium can with helium exchange gas (one atmosphere at room temperature). Data were collected on the Special Environment Powder Diffractometer (SEPD) at Argonne's Intense Pulsed Neutron Source.[10] The sample was cooled with a Displex closed cycle helium refrigerator (Air Products and Chemicals, Inc.). Data were collected at 23 temperatures from 19 K to 573 K in four separate experimental runs. In the first experiment, data were collected at 295, 250, 200, 150, 100, 50, and 19 K in that order.

Then, to carefully investigate the intermediate phase region which was suspected in the original data, additional data were collected from 250 K to 150 K in 10 K increments. Following the analysis of these data, it was clear that the transition from the intermediate phase to $R\bar{3}$ must be above room temperature. Thus, data were then collected with the sample in a simple furnace at 297 K, 413 K, and 573 K and at 345 K and 513 K in two runs separated by a few days.

As will be seen in the subsequent discussion of data analysis and results, the data from these four separate experiments were quantitatively consistent except for a small change in lattice constants between the first run and the other three runs. This effect is noticeable primarily as a small systematic shift in the hexagonal c-axis lattice constant in the $R\bar{3}$ phase and is attributed to the relaxation of residual strain in the sample which occurs only on the first temperature cycle below room temperature. The observed shift in lattice constant does not alter the conclusions drawn in this paper, but does support the hypothesis that the peak broadening which has been observed in nearly all powder diffraction data for Chevrel-phase systems is the result of residual strain.

DATA ANALYSIS

High resolution ($\Delta d/d \approx 0.0035$) data from the $2\theta = 150°$ detector banks of the SEPD were analyzed by the Rietveld technique[11] to obtain complete structural parameters at each temperature. The data above 175 K refined successfully in the $R\bar{3}$ rhombohedral space group. The refinements were done in the hexagonal setting which is most commonly used for reporting $R\bar{3}$ Chevrel-phase structures. For the $R\bar{3}$ structure, the refinements included 776 Bragg reflections for d-spacings from 0.64 Å to 3 Å and a total of 20 refineable

parameters (including two background parameters, extinction, absorption and a peak width parameter). In order to explore the large displacement perpendicular to the threefold axis that is common for the metal ion in the Chevrel phases, components of the anisotropic Debye-Waller factor were refined for Ba. The other atoms were refined with isotropic temperature factors. A plot of the raw data and the refined profile at 295 K is shown in Fig. 2.

The departure from $R\bar{3}$ symmetry was obvious in the raw data for temperatures below 175 K. Thus, refinements were attempted in the $P\bar{1}$ triclinic space group which is obtained by the loss of the threefold axis in the $R\bar{3}$ space group. The data at 150 K were the first to be refined with a $P\bar{1}$ model. Starting values for the atom positions were taken as the refined atom positions at 200 K expressed in rhombohedral coordinates. The transformation from hexagonal to rhombohedral coordinates is given by

$$\begin{bmatrix} x_R \\ y_R \\ z_R \end{bmatrix} = \begin{bmatrix} 1 & 0 & 1 \\ -1 & 1 & 1 \\ 0 & -1 & 1 \end{bmatrix} X \begin{bmatrix} x_H \\ y_H \\ z_H \end{bmatrix}. \qquad (1)$$

The rhombohedral lattice constants are given by

$$a_R = \frac{1}{3}\,(3a_H^2 + c_H^2)^{1/2} \qquad (2)$$

$$\sin\frac{\alpha_R}{2} = \frac{3}{2}\left[\left(\frac{c_H}{a_H}\right)^2 + 3\right]^{-1/2}. \qquad (3)$$

The starting lattice parameters for the initial triclinic refinement at 150 K were taken as the rhombohedral lattice parameters at 200 K with a increased by 1% and c decreased by 1% in order to remove the degeneracy by artificially introducing a small triclinic distortion. With this simple starting model, atom positions were fixed in the first refinement and the triclinic lattice constants were refined. Convergence to a stable solution was reached within a few cycles. The atom positions were then allowed to refine. These also converged within a few cycles. The stability and uniqueness of the solution was then tested by interchanging lattice parameters and by offsetting atom positions by several standard deviations. In every case, the refinement converged to the same solution within a few cycles. With such a small triclinic distortion, large correlations between atom positions might be expected. However, the correlations never exceeded 60%, and no problems were experienced in stability or convergence of the $P\bar{1}$ refinements.

The final $P\bar{1}$ triclinic refinements were based on 2306 Bragg reflections with d-spacings from 0.64 Å to 3 Å and included 37 refineable parameters. A single isotropic temperature factor was used for the three independent Mo atoms and another for the four independent S atoms. Tests where these constraints were relaxed indicated that this simplification of the model was justified. The anisotropic Debye-Waller factor of Ba was refined with two independent components rather than full triclinic symmetry which would require six components. This model assumes that the combined static and thermal displacement of Ba has essentially the same symmetry in the triclinic and rhombohedral phases. Physically, such an assumption could easily be violated. The Ba density could be cigar shaped in the triclinic phase rather than disc shaped as it must be by symmetry in the rhombohedral phase.

Unfortunately, attempts to refine the Ba Debye-Waller factor with full triclinic symmetry were inconclusive. The refinements converged, but large standard deviations made it impossible to extract any meaningful physics. Thus, the idealized, two-parameter model was used in order to learn as much as possible about the temperature dependence of the Ba static and thermal displacement in the triclinic structure. The raw data and refined profile at 19 K are plotted in Fig. 3.

Since no complete structural parameters have been published by others who have studied $BaMo_6S_8$, refined lattice constants, atom positions and temperature factors are given in Table I and Table II for the seven temperatures studied in the first experiment. In Table II, which describes the $P\bar{1}$ refinements, it should be noted that atoms Mo1, Mo2, and Mo3 correspond to Mo in the $R\bar{3}$ structure; atoms S1, S2, and S3 correspond to S1 and atom S4 corresponds to S2 in the $R\bar{3}$ structure. Complete refinement results for the other data can be obtained from the first author.

A comparison of the weighted profile R value (R_{wp}) to the expected R value based on statistics (R_{exp}) for all of the 23 refinements indicated very good agreement between the structural models and the experimental data. For all cases, R_{wp}/R_{exp} was less than 2, with 1.5 being a more typical value for the majority of the data sets. From these results, it is clear that the distortion of the $R\bar{3}$ structure in the region just above the rhombohedral-to-triclinic transition at 175 K is a rather subtle effect. The evidences for the existence of an intermediate phase are, nevertheless, quite clear upon careful examination of the data and comparison to the analogous distorted $R\bar{3}$ phase which has been previously observed in $PbMo_6S_8$ and $SnMo_6S_8$.[12]

Figure 4 shows the refined peak width parameter versus temperature. In the currently used Rietveld refinement code,[11] this parameter is proportional

to the root mean squared sum of the instrumental resolution resulting from geometrical considerations and the component of sample-contributed peak broadening which has a wavelength dependence consistent with isotropic strain. It is well known from previous powder diffraction studies of Chevrel-phase systems in this Laboratory that almost all of these materials show significant amounts of peak broadening which is thought to result from the existence of residual strain. This strain is introduced into the sintered samples because of the stresses which result from the highly anisotropic thermal expansion common to all Chevrel-phase materials. As previously mentioned, the strain can apparently be relaxed somewhat by thermal cycling as well as by thorough grinding of the sample, but may be impossible to eliminate.

The peak widths plotted versus temperature in Fig. 4 are predominantly due to the sample; the instrumental peak width in the same units is about 7. A smoothly increasing peak width with decreasing temperature would be expected as a result of the strain resulting from the anisotropic thermal expansion. However, the data in Fig. 4 show a sharply diverging peak width as the transition at 175 K is approached from higher temperatures. As will be seen later, this sharp increase in peak width is the result of the growth of satellite reflections on the shoulders of several of the original $R\bar{3}$ Bragg reflections and is, in fact, a mean width since the reflections which develop shoulders appear to be broadened more than is indicated in Fig. 4, while other peaks remain relatively sharp.

At temperatures below 175 K in the triclinic phase, the peak width suddenly drops to a lower value, suggesting that the transition relaxes internal strain, and then rises to a somewhat constant value. Thermal expansion anisotropy probably plays a less significant role in the triclinic

phase. The data of Fig. 4 also support the hypothesis that thermal cyling relaxes the internal strain to a small degree. The later runs consistently exhibit narrower peaks than the data taken upon decreasing temperature from 295 K to 19 K.

More direct evidence for the intermediate phase can be seen in a comparison of raw diffraction data to the best-fit Rietveld profiles based on an $R\bar{3}$ model. The pattern of peak broadening and the development of satellite reflections is identical to that observed in $PbMo_6S_8$ and $SnMo_6S_8$ at low temperature;[12] i.e., the satellite peaks develop around the same $R\bar{3}$ peaks as in the previous case. Figure 5 shows a small section of the raw data and best-fit profiles for an $R\bar{3}$ model for a series of temperatures above and just below 175 K. These plots are produced by refining the data with an $R\bar{3}$ model, but with the peak width parameter constrained to its room temperature value in order to emphasize the departure from an $R\bar{3}$ diffraction pattern. The progressive development of satellite peaks around some of the $R\bar{3}$ peaks, especially the 324 (hexagonal) peak at a d spacing of 1.564 Å, while other peaks remain sharp, is easily seen in these plots. It is also significant to note that the $R\bar{3}$ peaks which develop the most prominent satellites are those which split most dramatically in the triclinic phase below 175 K. However, the original $R\bar{3}$ peaks remain perfectly in position above 175 K, suggesting that the intermediate phase is a modulation of the $R\bar{3}$ structure and, more specifically, supporting the hypothesis that the same incommensurate modulation vector collapses to a commensurate value to produce the triclinic distortion.

The temperature range over which the intermediate phase exists is most evident in a plot of the hexagonal c axis versus temperature. As shown in Fig. 6, the c-axis thermal expansion is negative from 175 K to about 340 K and

positive for higher temperatures. The reversal in sign is abrupt, with the temperature dependence being nominally linear in the two regions. This is the same thermal expansion anomaly which signals the transition in $PbMo_6S_8$ and $SnMo_6S_8$ and is actually more pronounced in $BaMo_6S_8$ than in the other two systems.

From these diffraction data alone, it is probably not possible to unambiguously identify the structure which exists for $BaMo_6S_8$ between 175 K and 340 K. Previous attempts to solve the structure for the case of $PbMo_6S_8$ were not successful even though numerous possible models, primarily subgroups and supercells of $R\bar{3}$ were tried. If the satellites were well-separated, indexing might be possible. Unfortunately, sample-contributed strain broadening makes it impossible to resolve the satellites even if higher instrumental resolution was employed.

A knowledge of the structures of the phases below 175 K and above 340 K does allow Landau theory to be applied to determine what intermediate structures are possible if it is assumed that the transitions are displacive. For this analysis, it is important to know the details of the triclinic distortion below 175 K.

Within the precision of this measurement, the triclinic distortion of the unit cell appears to be continuous. The lattice parameters as a function of temperature are plotted in Figs. 7 and 8. [For the $R\bar{3}$ phase, the equivalent rhombohedral values according to Eqs. (2) and (3) are plotted.] The small shift in lattice parameters (presumably due to relaxation of residual strain) between the first and subsequent low temperature runs is visible in these plots, but does not alter the conclusions. The total triclinic distortion of the cell is in reasonable agreement with that reported by Baillif et al.[1] However, allowing for the different setting of the axes, unit cell angles β

and γ appear to be interchanged from the (corresponding) values reported by Baillif et al. Repeated efforts to achieve convergence with a cell equivalent to that previously reported were unsuccessful. The refinement always returned to the same solution. It should be noted that the high resolution powder data are particularly sensitive to unit cell parameters and convergence to a false minimum is highly unlikely for a cell distortion this large. One possible explanation for the discrepancy between the two reported unit cells is that the samples actually differ with respect to defect concentration. It is well established that impurity defects in the $R\bar{3}$ Chevrel-phase structure can alter the unit cell dimensions in an anisotropic way.[13,14]

The unit-cell volume as a function of temperature is plotted in Fig. 6. The unusual curvature in the volume vs. temperature curve in the triclinic phase may result from a rapidly changing electronic contribution to the free energy. From these data, it is impossible to detect a finite volume discontinuity at the transition. Based on the error bars for the refined cell volume, an upper limit for the volume discontinuity at the transition would be about 0.02 $Å^3$.

A small positive volume change would be in agreement with the decrease of the transition temperature with increasing pressure previously reported.[9] Based on the data of Hor et al.[5] for 1 bar and 4 kbar, $(\partial T_s/\partial P)_{P=0} \cong$ 4 K/kbar. The Clapeyron equation, $(\partial P/\partial T_s) = L/(T\Delta V)$, can be used to estimate the latent heat, L, of the transition where $T_s(P)$ is the temperature of the structural transition at pressure P. Taking a value of 0.02 $Å^3$ as an upper limit for ΔV, L = 53 J/g-at. This is in reasonable agreement with the specific heat data of Lachal, et al.[2], and is close to the reported value, 46 J/g-at, for $EuMo_6S_8$.[3] (A value for the latent heat of the transition in $BaMo_6S_8$ has not been reported.) A more precise estimate of the volume change

at the transition is not possible by this technique.

The distortion of the Mo_6S_8 cluster-framework associated with the transition is illustrated in Fig. 10. The axial sulfur atoms (S4 in the $P\bar{1}$ structure) move off the original threefold axis such that two of the S4-Mo bonds (S4-Mo2 and S4-Mo3) are shortened and one (S4-Mo1) is lengthened by 2%. In a previously equilateral triangle of Mo atoms, one Mo-Mo bond (Mo2-Mo3) is lengthened while the other two are shortened by about 1.4%. The two Mo1-Mo2-Mo3 triangles also follow their respective capping S4 atoms to some extent, resulting in a small shear of the overall cluster. The Mo-S intercluster bonds (e.g., Mo1-S1' in Fig. 10) show a similar magnitude of distortion, with two becoming longer and one becoming shorter than in the $R\bar{3}$ structure.

A partial list of atom-atom distances versus temperature for the data included in Tables I and II is given in Table III. From these data it is clear that the magnitude of the distortion is nominally the same at all temperatures in the triclinic phase. The 160 K and 170 K data (not included in this Table) also support this conclusion, suggesting that the transition is first-order. The Ba-S4 distances indicate a possible explanation for the displacement of the axial sulfur atoms off the original threefold axis. The Ba-S4 distance (using the $P\bar{1}$ atom-naming convention) is constant at 2.93Å in the $R\bar{3}$ structure but increases to 2.97(2)Å in the $P\bar{1}$ structure at 19 K allowing the Ba atom to occupy the origin position. Previous work on $YbMo_6S_8$ has suggested that the metal ion in the $R\bar{3}$ Chevrel-phase structure is statically displaced from the origin position by about 0.1 Å even at low temperature.[15] This delocalization of the metal ion from the origin is apparently common to all $R\bar{3}$ Chevrel-phase systems[16] and has even been observed at low temperature for the small Ho^{3+} ion in $HoMo_6S_8$.[17] Unusually short metal

ion to axial sulfur distances may be the explanation for this pronounced anisotropy.[18] The triclinic Chevrel-phase structures, where the axial sulfur atoms are displaced, may be the only cases in which the metal ion actually occupies the origin site.

Further evidence for this localization of the Ba ion to the origin at low temperature is provided by the basal plane component of the Debye-Waller factor from the structural refinements. The components of the anisotropic Debye-Waller tensor given in Table I show that Ba in the $R\bar{3}$ structure exhibits the pronounced anisotropy common to other Chevrel phase systems. Indeed, the refined axial component of the Debye-Waller tensor, b_{33}, is near zero and in one case is slightly negative. This anomalous behavior of the Debye-Waller tensor is common in refinements of this structure and is thought to be the result of applying a harmonic model to a markedly anharmonic system. Nevertheless, a useful approximation of the mean squared displacement perpendicular to the threefold axis in the $R\bar{3}$ structure is given by the b_{11} term according to the relation

$$\langle X_{\perp}^2 \rangle = b_{11}/2\pi^2 a^{*2} = b_{11} a^2 \sin^2 120°/2\pi^2. \qquad (4)$$

For the triclinic structure, as previously discussed, the Debye-Waller tensor has been constrained as if the symmetry were rhombohedral, giving only two independent refineable components, b_{11} and b_{12}. Since the unit cell is actually nearly cubic, the displacement perpendicular to the [111] axis can be approximated by

$$\langle X_{\perp}^2 \rangle = (b_{11} - b_{12})\, \bar{a}^{-2}/2\pi^2 \qquad (5)$$

where $\bar{a} = (a+b+c)/3$. Comparison of this approximation with a rigorous diagonalization of the Debye-Waller tensor shows that, for this system, the approximation is accurate within the standard deviations of the measurement.

The mean squared perpendicular displacement of the Ba ion as a function of temperature is plotted in Fig. 11. The shallow slope of the points in the $R\bar{3}$ phase is comparable to that observed in $YbMo_6S_8$[15] and implies that a static delocalization would be present at low temperature if the $R\bar{3}$ to $P\bar{1}$ transition did not occur. In the $P\bar{1}$ phase, however, the mean squared displacement decreases as expected with decreasing temperature, indicating no significant static displacement of the Ba ion at low temperature. The observations suggest that the transition from rhombohedral to triclinic is accompanied by a disorder-order transition of the Ba ion. In the triclinic phase, the Ba ion is able to order on a localized site at the origin of the unit cell because the axial sulfur atoms are shifted off the [111] axis. This is in contrast to the $R\bar{3}$ Chevrel-phase structures where the metal ion appears to be spatially disordered around the threefold axis at low temperature. Whether an ordered modulation of the Ba ion displacement is present in the intermediate phase of $BaMo_6S_8$ remains an open question.

THEORY

A knowledge of the atom displacements associated with the triclinic distortion of $BaMo_6S_8$ below 175 K allows an extended Landau theory to be applied in order to determine whether the observed atom displacements can be the result of any possible transition induced by a single order parameter. Such an analysis shows that the observed displacements are not consistent with any of the possible order parameters which induce transitions from $R\bar{3}$ with no change in unit cell volume. These results support the experimental

observation that the phase immediately above 175 K is not a commensurate $R\bar{3}$ structure.

One of the essential features of the Landau theory[19] of phase transitions is the existence of an order parameter which induces the transition. The order parameter is zero in the high symmetry phase and nonzero in the low symmetry phase. The components of the order parameter are the contributions of the basis functions for the irreducible representation of the high symmetry space group. Often the order parameter is a lattice displacement corresponding to a soft mode. However, the formulation includes the possibilities of site occupation or site orientation as in order-disorder transitions, electric or magnetic dipole ordering as in ferroelectric or ferromagnetic transitions, orientational-positional ordering as in liquid crystals, etc. In one approach[19] the lower symmetry phase is obtained by minimization of the thermodynamic potential. Recently, the possible lower symmetry commensurate phases were obtained[20] for the 230 space groups by group theoretical methods. These methods bypass the unsystematic and often difficult minimization process. Moreover, the group theoretical approach is an extension of the Landau theory in that it includes lower symmetry phases obtained by either continuous or discontinuous transitions. The lower symmetry phases are thus all those that can be induced by a single order parameter.

The possible phases for the group of interest here, $R\bar{3}$, are listed in Table IV.[21] The labeling of $\vec{k}$ vectors and the associated representations follows that of Ref. 22. Those transitions that are allowed to be continuous within the Landau theory are indicated by an asterisk. Only order parameters whose contributions are basis functions of space group representations with $\vec{k}$ a point of symmetry[23] are listed. Only these points can induce

commensurate transitions and, thus, for $R\bar{3}$ only the four points Γ, T, L, and F need to be considered. Transitions which preserve the unit cell size, as well as changes of order 2, 4, and 8, are induced from $R\bar{3}$ and are listed in Table IV.

Transitions from $R\bar{3}$ which preserve the unit cell volume are obtained from $\vec{k} = 0$, the Γ point of the Brillonin zone. These transitions are discussed in detail since structural refinement confirms the equitranslational nature of the $P\bar{1}$ phase below 175 K. Also, so that the essential arguments can be seen more clearly, attention is focussed on the distortions of the molybdenum (Mo) atoms labeled 1, 2, 3 and 1', 2', 3' in Fig. 10.

The crystal is taken to be a system of rN atoms at positions $\vec{R} + \vec{d}$. The set $\{\vec{R}\}$ labels Bravais lattice points which will be finite (N points) under periodic boundary conditions. $\vec{d}$ labels one of the r basis atoms in the unit cell. For $BaMo_6S_8$, there are 15 basis atoms in the unit cell. A 3rN dimensional basis of elementary displacements can be defined as $\hat{e}_\alpha(\vec{R},\vec{d})$. Here $\alpha = 1, 2, 3$ with $\vec{R}$ taking on N values and $\vec{d}$ taking on r values. $\hat{e}_\alpha(\vec{R}, \vec{d})$ is the displacement at $\vec{R} + \vec{d}$ in the $\alpha = 1, 2, 3$ $(\hat{i},\hat{j},\hat{k})$ direction. The effect of a space group symmetry transformation $g = (S|\vec{t} + \vec{\tau})$ on the elementary displacement is

$$(S|\vec{t} + \vec{\tau})\ \hat{e}_\alpha(\vec{R},\vec{d}) = \sum_\beta V_{\beta\alpha}(S)\ \hat{e}_\beta(\vec{R}_g,\vec{d}_g)$$

$$= \sum_{\beta R' d'} V_{\beta\alpha}(S)\ \hat{e}_\beta(\vec{R},\vec{d}')\ \delta(\vec{R}' - \vec{R}_g)\ \delta(\vec{d}' - \vec{d}_g) \qquad (6)$$

where

$$\vec{d}_g = (S|\vec{\tau})^{-1}\,\vec{d} - \vec{R}_d(s),$$

$$\vec{R}_g = (S|\vec{\tau})^{-1}\,\vec{R} + \vec{R}_d(s)$$

and $V_{\beta\alpha}(S)$ are the usual components of the matrix of rotation S in $\hat{i},\hat{j},\hat{k}$. $\vec{R}_d(s)$ is the primitive translation needed to take $(S|\vec{\tau})^{-1}\vec{d}$ back into the original unit cell. The matrix transformation on the displacements is then

$$T^{d'd}_{\beta R',\alpha R}(g) = S_{\beta\alpha}\,\delta(\vec{R}' - \vec{R}_g)\,\delta(\vec{d}' - \vec{d}_g). \tag{7}$$

The displacements carry a representation of the high symmetry space group which is in general reducible. Maradudin and Vosko[24] have shown that a multiplier representation, in general reducible, of the little cogroup can be obtained from Eq. (7) and the matrix elements are of the general form

$$T^{d'd}_{\beta\alpha}(\vec{k},S) = \delta(R' - R_g)\,\delta(\vec{d}' - \vec{d}_g)$$

$$\exp\{i\,\vec{k}\cdot(\vec{d}' - S\vec{d})\}\,S_{\beta\alpha}. \tag{8}$$

Here S denotes an element of the little cogroup. This representation will induce representations which transform under lattice translations $\vec{t}$ as $e^{i\,\vec{k}\cdot\vec{t}}$, i.e., lattice modes with periodicity determined by $\vec{k}$.

For the Γ point the argument of the exponential is always zero and the little cogroup is C_{3i}. Moreover, the displacements are repeated in each unit cell so that there will be no unit cell change. That portion of the matrix $T(\vec{k},S)$, Eq. (8), corresponding to Mo atoms 1, 2, 3, 1′, 2′, and 3′ (in that order) is given in Table V. Thus the d′d block of $T(\Gamma,S)$ is positioned as in

Table V and the $\beta\alpha$ component within that block is obtained from the usual matrices S which follow:

$$E = \begin{pmatrix} 1 & 0 & 0 \\ 0 & 1 & 0 \\ 0 & 0 & 1 \end{pmatrix}, \quad I = \begin{pmatrix} -1 & 0 & 0 \\ 0 & -1 & 0 \\ 0 & 0 & -1 \end{pmatrix}, \quad C_3^+ = \begin{pmatrix} -1/2 & -\gamma & 0 \\ \gamma & -1/2 & 0 \\ 0 & 0 & 1 \end{pmatrix} \tag{9}$$

$$C_3^- = \begin{pmatrix} -1/2 & \gamma & 0 \\ -\gamma & -1/2 & 0 \\ 0 & 0 & 1 \end{pmatrix}, \quad S_6^+ = \begin{pmatrix} 1/2 & -\gamma & 0 \\ \gamma & 1/2 & 0 \\ 0 & 0 & -1 \end{pmatrix}, \quad S_6^- = \begin{pmatrix} 1/2 & \gamma & 0 \\ -\gamma & 1/2 & 0 \\ 0 & 0 & -1 \end{pmatrix}$$

with $\gamma = \frac{\sqrt{3}}{2}$. The full matrices $T(\Gamma, S)$ are 45 x 45 dimensional matrices. This representation contains irreps of the little cogroup C_{3i}. The irreps of C_{3i} are listed in explicit form in Table VI. Since $\vec{k} = 0$ the irreps of C_{3i} also form irreps of the entire space group $R\bar{3}$. Usual group theoretical methods [25] allow the number of times (subduction frequency) that each irrep is contained in the displacement representation to be calculated. The subduction frequencies are

$$i(\Gamma_1^+) = 7,$$

$$i(\Gamma_1^-) = 8,$$

$$i(\Gamma_2^+ + \Gamma_3^+) = 14,$$

$$i(\Gamma_2^- + \Gamma_3^-) = 16.$$

A phase transition is induced by a particular order parameter, i.e., irrep of $R\bar{3}$. The calculations which follow will focus on the $\Gamma_2^+ + \Gamma_3^+$ irrep. It induces the transition to $P\bar{1}$, which must be discontinuous. One would therefore like to consider those displacements which are the basis functions for this irrep. Group theory provides a procedure for obtaining these functions which makes use of projection operators.[25] The general form for these operators is

$$P_{ij}^{(m)} = \frac{N_m}{|\bar{G}^{\vec{k}}|} \sum_{S\varepsilon \; \bar{G}^{\vec{k}}} \Gamma_{ij}^{m}(s)^* \, O_s \tag{10}$$

where m numbers one of the irreps of the little cogroup $\bar{G}^{\vec{k}}$. For the little cogroup $\bar{G}^{\Gamma}$, which specifically is C_{3i}, the irrep $\Gamma_2^+ + \Gamma_3^+$, or the third irrep (m = 3), gives the projection operators

$$P_{11}^{(3)} = T(\Gamma,E) + T(\Gamma,I) - \frac{1}{2}[T(\Gamma,C_3^+) + T(\Gamma,C_3^-) + T(\Gamma,S_6^+) + T(\Gamma,S_6^-)] \tag{11}$$

$$P_{21}^{(3)} = \gamma[-T(\Gamma,C_3^+) + T(\Gamma,D_3^-) + T(\Gamma,S_6^+) - T(\Gamma,S_6^-)]$$

These projection operators are listed in Table VII. The restriction to the Mo atoms is seen to be a valid simplification, since the operators will not

couple these atomic displacements to any others. These two operators taken together will then select displacements of the Mo atoms which transform as basis functions of the $\Gamma_2^+ + \Gamma_3^+$ irrep. The z displacements of the Mo atoms are also taken to be zero since they are not coupled to the x-y displacements. A general x-y displacement from the $R\vec{3}$ symmetry locations for the Mo atoms can be written as $\vec{\psi} = [. \ . \ . \ . \ x_1, y_1, 0, x_2, y_2, 0, x_3, y_3, 0, . \ . \ . \ .]$. One then allows $P_{11}^{(S)}$ to act on $\vec{\psi}$ (as a column vector) and obtain a projected vector with components $\psi_{11}^{(3)} = [. \ . \ . \ .a, b, 0, c, d, 0, e, f, 0, . \ . \ .]$.

This results in a set of six equations,

$$
\begin{aligned}
&x_1 + \tfrac{1}{4} x_2 + \tfrac{\gamma}{2} y_2 + \tfrac{1}{4} +_3 - \tfrac{\gamma}{2} y_3 = a \\
&y_1 - \tfrac{\gamma}{2} x_2 + \tfrac{1}{4} y_2 + \tfrac{\gamma}{2} x_3 + \tfrac{1}{4} y_3 = b \\
&\tfrac{1}{4} x_1 - \tfrac{\gamma}{2} y_1 + x_2 + \tfrac{1}{4} x_3 + \tfrac{\gamma}{2} y_3 = c \\
&\tfrac{\gamma}{2} x_1 + \tfrac{1}{4} y_1 + y_2 - \tfrac{\gamma}{2} x_3 + \tfrac{1}{4} y_3 = d \\
&\tfrac{1}{4} x_1 + \tfrac{\gamma}{2} y_1 + \tfrac{1}{4} x_2 - \tfrac{\gamma}{2} y_2 + x_3 = e \\
&-\tfrac{\gamma}{2} x_1 + \tfrac{1}{4} y_1 + \tfrac{\gamma}{2} x_2 + \tfrac{1}{4} y_2 + y_3 = f,
\end{aligned}
\qquad (12)
$$

determining symmetry restricted displacements of a,b,c,d,e, and f, for x_1, y_1 x_2, y_2, x_3, and y_3. Notice that any solution for a,b,c,d,e,f will imply by $P_{11}^{(3)}$ of Table VII that atoms 1′, 2′, 3′ will have opposite displacements. Initially (at 200 K) the Mo atoms form an equilateral triangle of length 2.658 Å. The 150 K phase gives bond lengths of 2.63 Å, 2.63 Å, and

2.71 Å. Letting x_1^0 be the 200 K position of the Mo1 atom and a the displacement from x_1^0 for the 150 K phase and similarly for the other components, one can write

$$[(x_1^0 + a) - (x_2^0 + c)]^2 + [(y_1^0 + b) - (y_2^0 + d)]^2 = 2.63^2.$$

Knowing the initial positions of Mo1, Mo2, and Mo3, one obtains

$$(a - c + \gamma)^2 + (b - d + \frac{3}{2})^2 = 3(\frac{2.63}{2.658})^2 \tag{13}$$

$$(e - a + \gamma)^2 + (b - f + \frac{3}{2})^2 = 3\,(\frac{2.63}{2.658})^2 \tag{14}$$

$$(e - c + 2\gamma)^2 + (f - d)^2 = 3\,(\frac{2.71}{2.658})^2\ . \tag{15}$$

From Eq. (12), e and f can be expressed in terms of a, b, c, and d as

$$e = \frac{a}{2} + \gamma b + \frac{c}{2} - \gamma d \tag{16}$$

$$f = -\gamma a + \frac{b}{2} + \gamma c + \frac{d}{2}\ . \tag{17}$$

Substituting for e and f in Eqs. (14) and (15), one obtains the result that the left side of each is the same. The left side of either can be written

$$a^2 + b^2 + c^2 + d^2 - 2(ac + bd) + 2\gamma(a - c) + 3(b - d) + 3.$$

Since the right sides of Eqs. (14) and (15) are not equal, one must conclude that $P_{11}^{(3)}$ projects out a displacement which does not transform as observed in

the experiment.

The same procedure can be followed for $P_{21}^{(3)}$ to obtain

$$c = \frac{a}{2} - \gamma b + \frac{e}{2} + \gamma f \tag{18}$$

$$d = \gamma a + \frac{b}{2} + \gamma e + \frac{f}{2} . \tag{19}$$

Inserting these equations into Eqs. (13) and (15) again leads to the same inconsistency. Thus one concludes that the transition induced by $\Gamma_2^+ + \Gamma_3^+$ does not allow the Mo atoms to move as observed.

There are three other irreps which can be considered. It can be seen in a similar fashion that this set of basis functions is again inconsistent with experiment. In particular, the $\Gamma_2^- + \Gamma_3^-$ irrep yields the same detailed results as $\Gamma_2^+ + \Gamma_3^+$ for the Mo atoms. This inconsistency is obtained for each of the Γ point irreps.

Based on these extended Landau theory considerations, it must be assumed that either the high or low temperature structures are incorrectly determined or that an intermediate phase exists. Even though the experimental data indicated the existence of an intermediate phase, several other structural models for the low temperature phase were investigated. As previously shown (Table IV) the possible displacive transitions from $R\bar{3}$ to lower symmetry include P1 and $P\bar{1}$ cells with doubled cell volumes, as well as R3 and $R\bar{3}$ cells with two, four, and eight times the original volume. Attempts to fit the low temperature $BaMo_6S_8$ data with several of these models were not successful. Although it is not possible to claim that the search for models which fit the data has been exhaustive, these efforts support the conclusion that the low temperature structure of $BaMo_6S_8$ is triclinic, $P\bar{1}$, with no increase in cell

volume. Since it is often difficult to differentiate between $P\bar{1}$ and P1 from diffraction data, P1 must also be included as a possible solution. (P1 refinements were, in fact, attempted but always converged toward the $P\bar{1}$ solution.)

Assuming that the high and low temperature structures of $BaMo_6S_8$ are correctly known, the extended Landau theory analysis requires that the phase immediately above 175 K is not a commensurate $R\bar{3}$ structure, but is a structure induced from the $R\bar{3}$ structure which exists above 340 K. A structural model for the intermediate phase which is consistent with both theory and experiment is an incommensurate modulation of the $R\bar{3}$ structure. The incommensurate modulation appears upon decreasing temperature at 340 K and eventually locks in as a commensurate wave vector to produce the observed triclinic distortion at 175 K.

CONCLUSIONS

Both theory and experiment support the existence of an intermediate phase between the high-temperature rhombohedral $R\bar{3}$ and low-temperature triclinic $P\bar{1}$ (or P1) phases of $BaMo_6S_8$. The diffraction data for $BaMo_6S_8$ in this intermediate phase region show a pattern of satellite reflections identical to that recently observed at low temperature in $PbMo_6S_8$ and $SnMo_6S_8$. In all three systems, the transition from $R\bar{3}$ into the modulated (or distorted) $R\bar{3}$ phase is signaled by an abrupt reversal of the sign of the hexagonal c-axis thermal expansion. These results suggest that, although the structure of this phase has not been unambiguously determined, the same structure is present in all three systems.

It is logical to assume that this sequence of phase transitions is common to all Chevrel-phase systems. In particular, the same intermediate phase

should be present in other systems where the $P\bar{1}$ structure has been reported to exist at low temperature, e.g., $EuMo_6S_8$. Furthermore, these results also imply that the sudden onset of superconductivity observed at high pressure in $BaMo_6S_8$ and $EuMo_6S_8$ is caused by a transition from the triclinic structure into a modulated $R\bar{3}$ structure, rather than the simple $R\bar{3}$ structure present at high temperatures.

It is significant to note that the highest superconducting transition temperatures observed in the Chevrel phases are for materials which possess the modulated $R\bar{3}$ structure. One possible explanation for this is that unusually soft phonons associated with the modulation enhance T_c.

REFERENCES

1. R. Baillif, A. Dunand, J. Muller and K. Yvon, Phys. Rev. Lett. 47, 672 (1981).

2. B. Lachal, R. Baillif, A. Junod and J. Muller, Solid State Commun. 45, 849 (1983).

3. B. Baillif, A. Junod, B. Lachal, J. Muller and K. Yvon, Solid State Commun. 40, 603 (1981).

4. H. Nohl, W. Klose and O. K. Anderson, in "Superconductivity in Ternary Compounds I," edited by Ø. Fischer and M. B. Maple (Springer-Verlag, 1982) p. 165.

5. P. H. Hor, M. K. Wu, T. H. Lin, X. Y. Shao, X. C. Jin, and C. W. Chu, Solid State Commun. 44, 1605 (1982).

6. D. W. Harrison, K. C. Lim, J. D. Thompson, C. Y. Huang, P. D. Hambourger and H. L. Luo, Phys. Rev. Lett. 46, 280 (1981).

7. C. W. Chu, S. Z. Huang, C. H. Lin, R. L. Meng, M. K. Wu and P. H. Schmidt, Phys. Rev. Lett. 46, 276 (1981).

8. M. Decroux, M. S. Torikachvili, M. B. Maple, R. Baillif, Ø. Fischer and J. Muller, Phys. Rev. B28, 6270 (1983).

9. W. Kalsbach, Ber. Kernforschungsanlage Juelich, (Juel-1921), 85 (1984).

10. J. D. Jorgensen and J. Faber, Jr. in "Proceedings of the Sixth Meeting of the International Collaboration on Advanced Neutron Sources," (Argonne National Laboratory, ANL-82-80, 1983) p. 105.

11. R. B. VonDreele, J. D. Jorgensen and C. G. Windsor, J. Appl. Crystallogr. 15, 581 (1982).

12. J. D. Jorgensen and D. G. Hinks, Solid State Commun. 53, 289 (1985).

13. J. D. Jorgensen, D. G. Hinks and F. J. Rotella, in "Ternary Superconductors," edited by G. K. Shenoy, B. D. Dunlap and F. Y. Fradin (Elsevier North Holland, 1981) p. 69.

14. D. G. Hinks, J. D. Jorgensen and H.-C. Li, Phys. Rev. Lett. 51, 1911 (1983).

15. J. D. Jorgensen, D. G. Hinks, D. R. Noakes, P. J. Viccaro and G. K. Shenoy, Phys. Rev. B27, 1465 (1983).

16. K. Yvon, Solid State Commun. 25, 327 (1978).

17. J. D. Jorgensen and D. G. Hinks, unpublished.

18. J. D. Corbett, J. Solid State Chem. 39, 56 (1981).

19. L. D. Landau, Zh. Eksp. Teor. Fiz. 7, 19, 627 (1937); L. D. Landau and E. M. Lifshitz, Statistical Physics, 3rd ed. (Pergamon, New York, 1980).

20. D. M. Hatch, Lecture Notes in Physics, Vol. 201, G. Denardo, G. Ghirardi, and T. Weber, eds. (Springer, New York, 1984), 390; H. T. Stokes and D. M. Hatch, Phys. Rev. B. 30, 4962 (1984).

21. H. T. Stokes and D. M. Hatch, to be published.

22. A. P. Cracknell, B. L. Davies, S. C. Miller, and W. F. Love, Kronecker Product Tables, (IFI/Plenum, New York, 1979).

23. C. J. Bradley and A. P. Cracknell, The Mathematical Theory of Symmetry in Solids, (Clarendon, Oxford, 1972).

24. A. A. Maradudin and S. H. Vosko, Rev. Mod. Phys. 40, 1 (1968).

25. J. F. Cornwell, Group Theory in Physics, (Academic, New York, 1984).

TABLE I. Structural parameters for $BaMo_6S_8$ at 295 K, 250 K and 200 K in the $R\bar{3}$ rhombohedral space group (hexagonal setting). Numbers in parentheses are standard deviations of the last significant digit. The temperature factor for Ba has the form $\exp[-h^2b_{11}-k^2b_{22}-\ell^2b_{33}-2hkb_{12}-2h\ell b_{13}-2k\ell b_{23}]$ with the constraints $b_{11}=b_{22}=2b_{12}$, $b_{13}=b_{23}=0$.

	295 K	250 K	200 K
a(Å)	9.2974(2)	9.2939(2)	9.2897(3)
c(Å)	11.7734(4)	11.7741(5)	11.7752(6)
V(Å^3)	881.36(3)	880.75(3)	880.04(4)
x=y=z(Ba)	0	0	0
b_{11}(Ba)	0.0055(4)	0.0050(5)	0.0048(5)
b_{33}(Ba)	0.0000(2)	0.0003(2)	-0.0004(2)
x(Mo)	0.0125(2)	0.0125(2)	0.0125(2)
y(Mo)	0.1709(2)	0.1708(2)	0.1711(2)
z(Mo)	0.4064(1)	0.4064(1)	0.4065(1)
B(Mo)	0.55(3)	0.56(3)	0.48(4)
x(S1)	0.3207(4)	0.3212(4)	0.3212(4)
y(S1)	0.2937(3)	0.2939(4)	0.2934(4)
z(S1)	0.4160(3)	0.4162(3)	0.4157(3)
B(S1)	0.69(5)	0.66(6)	0.49(6)
x=y(S2)	0	0	0
z(S2)	0.2490(5)	0.2492(5)	0.2494(6)
B(S2)	0.78(8)	0.70(9)	0.44(9)
R_{wp}	0.049	0.055	0.061
R_{exp}	0.031	0.038	0.040

TABLE II. Structural parameters for $BaMo_6S_8$ at 150 K, 100 K, 50 K and 19 K in the $P\bar{1}$ triclinic space group. The anisotroic temperature factor for Ba has the form stated in the caption of Table I with the constraints $b_{11}=b_{22}=b_{33}$, $b_{12}=b_{13}=b_{23}$

	150 K	100 K	50 K	19 K
a(Å)	6.6819(6)	6.6957(5)	6.6972(5)	6.6976(4)
b(Å)	6.6517(6)	6.6531(5)	6.6542(5)	6.6545(5)
c(Å)	6.5989(4)	6.5762(4)	6.5701(4)	6.5685(4)
α(°)	88.196(6)	88.004(6)	87.941(6)	87.929(5)
β(°)	88.899(6)	88.978(5)	88.986(5)	88.978(5)
γ(°)	88.818(7)	88.868(6)	88.879(6)	88.887(5)
V(Å^3)	293.03(2)	292.67(2)	292.51(2)	292.46(2)
Ba: x=y=z	0	0	0	0
Mo1: x	0.4193(8)	0.4217(7)	0.4200(7)	0.4207(6)
y	0.5640(8)	0.5639(7)	0.5640(7)	0.5645(6)
z	0.2420(7)	0.2413(6)	0.2415(6)	0.2408(5)
Mo2: x	0.5631(8)	0.5638(7)	0.5638(6)	0.5640(6)
y	0.2312(7)	0.2338(6)	0.2327(6)	0.2330(5)
z	0.4163(7)	0.4161(7)	0.4162(6)	0.4166(6)
Mo3: x	0.2334(7)	0.2311(6)	0.2318(6)	0.2311(5)
y	0.4210(8)	0.4182(7)	0.4195(7)	0.4181(6)
z	0.5680(8)	0.5665(7)	0.5662(7)	0.5670(6)
S1: x	0.7380(16)	0.7381(15)	0.7389(14)	0.7381(13)
y	0.3942(16)	0.3921(14)	0.3952(14)	0.3936(13)
z	0.1196(15)	0.1233(13)	0.1215(13)	0.1237(12)
S2: x	0.3822(16)	0.3824(14)	0.3822(13)	0.3830(12)
y	0.1252(16)	0.1247(14)	0.1248(13)	0.1251(12)
z	0.7387(14)	0.7397(13)	0.7408(12)	0.7417(11)
S3: x	0.1224(17)	0.1179(15)	0.1197(14)	0.1191(13)
y	0.7351(17)	0.7341(16)	0.7324(16)	0.7319(14)
z	0.3861(15)	0.3885(14)	0.3871(13)	0.3875(12)
S4: x	0.2506(16)	0.2475(14)	0.2486(13)	0.2480(12)
y	0.2431(12)	0.2434(12)	0.2425(11)	0.2439(10)
z	0.2543(16)	0.2605(15)	0.2613(14)	0.2616(13)
b_{11}(Ba)	0.0038(5)	0.0024(5)	0.0014(4)	0.0012(4)
b_{12}(Ba)	-0.0023(4)	-0.0014(4)	-0.0007(4)	-0.0004(13)
B(Mo)	0.33(3)	0.25(3)	0.22(3)	0.16(3)
B(S)	0.38(5)	0.27(5)	0.22(5)	0.19(5)
R_{wp}	0.051	0.053	0.053	0.049
R_{exp}	0.030	0.033	0.035	0.030

TABLE III. Atom-atom distances in $BaMo_6S_8$ versus temperature. Atom labels match Fig. 6. Primed atom are related to unprimed atoms by inversion through the origin.

Atom 1	Atom 2	295 K	250 K	200 K	150 K	100 K	50 K	19 K
Ba	S1	3.201(3)	3.198(3)	3.192(4)	3.23(2)	3.23(2)	3.25(2)	3.24(2)
	S2				3.17(2)	3.16(2)	3.16(2)	3.16(2)
	S3				3.16(2)	3.16(2)	3.16(2)	3.16(2)
	S4	2.932(5)	2.934(6)	2.937(7)	2.94(2)	2.95(2)	2.95(2)	2.96(2)
Mo-Mo intracluster								
Mo1	Mo2	2.657(3)	2.654(3)	2.658(3)	2.63(2)	2.61(2)	2.62(2)	2.63(1)
	Mo2'	2.686(2)	2.685(3)	2.684(3)	2.68(2)	2.67(2)	2.67(2)	2.67(1)
	Mo3				2.63(2)	2.64(2)	2.62(2)	2.64(1)
	Mo3'				2.66(2)	2.67(2)	2.68(2)	2.68(2)
Mo2	Mo3				2.71(2)	2.71(2)	2.71(2)	2.71(2)
	Mo3'				2.71(2)	2.72(2)	2.72(2)	2.73(1)
Mo-Mo intercluster								
Mo1	Mo1'	3.411(3)	3.412(3)	3.409(3)	3.48(2)	3.45(2)	3.46(2)	3.45(2)
Mo2	Mo2'				3.35(2)	3.38(2)	3.37(2)	3.37(2)
Mo3	Mo3'				3.40(2)	3.38(2)	3.37(2)	3.37(2)
Mo-Mo cluster diagonals								
Mo1	Mo1'	3.778(3)	3.775(3)	3.778(4)	3.66(2)	3.65(2)	3.65(2)	3.65(2)
Mo2	Mo2'				3.85(2)	3.82(2)	3.84(2)	3.83(2)
Mo3	Mo3'				3.82(3)	3.86(3)	3.85(3)	3.86(2)

Mo-S intracluster								
S1	Mo1	2.501(4)	2.504(4)	2.504(4)	2.52(2)	2.51(2)	2.52(2)	2.51(2)
	Mo2	2.470(3)	2.471(4)	2.465(4)	2.49(2)	2.45(2)	2.47(2)	2.45(1)
	Mo3'	2.479(3)	2.479(3)	2.480(4)	2.45(2)	2.45(2)	2.44(2)	2.44(2)
S2	Mo1'				2.49(2)	2.48(2)	2.49(2)	2.48(2)
	Mo2				2.52(2)	2.52(2)	2.52(2)	2.53(1)
	Mo3				2.44(2)	2.44(2)	2.45(2)	2.44(1)
S3	Mo1				2.46(2)	2.50(2)	2.48(2)	2.48(2)
	Mo2'				2.51(2)	2.53(2)	2.52(2)	2.52(2)
	Mo3				2.48(2)	2.48(2)	2.46(2)	2.47(2)
S4	Mo1	2.405(5)	2.403(5)	2.403(6)	2.43(2)	2.45(2)	2.45(2)	2.45(1)
	Mo2				2.36(2)	2.37(2)	2.36(2)	2.36(2)
	Mo3				2.42(2)	2.36(2)	2.36(2)	2.35(2)
Mo-S intercluster								
S1	Mo1'	2.624(3)	2.626(3)	2.624(3)	2.63(2)	2.65(2)	2.63(2)	2.64(2)
S2	Mo2'				2.63(2)	2.64(2)	2.64(2)	2.65(2)
S3	Mo3'				2.62(2)	2.57(2)	2.59(2)	2.58(2)

TABLE IV

$\vec{k}$	Irrep	Dim	Lan	Lif	Size	G	$\vec{a}_1,\vec{a}_2,\vec{a}_3$	$\vec{v}$
Γ	1+	1	1	0	1	C3I-2	(1,0,0)(0,1,0)(0,0,1)	(0,0,0)
Γ	1-	1	0	0	1	*C3-4	(1,0 0)(0,1,0)(0,0,1)	(0,0,0)
Γ	2+3+	2	2	0	1	CI-1	(1,0,0)(0,1,0)(0 0 1)	(0,0,0)
Γ	2-3-	2	0	0	1	*C1-1	(1,0,0)(0,1,0)(0,0,1)	(0,0,0)
T	1+	1	0	0	2	*C3I-2	(0,1,1)(1,0,1)(1,1,0)	(0,0,0)
T	2+3+	2	0	0	2	*CI-1	(1,-1,0)(1,1,0)(1,0,1)	(0,0,0)
T	1-	1	0	0	2	*C3I-2	(0,1,1)(1,0,1(1,1,0)	(1/2,1/2,1/2)
T	2-3-	2	0	0	2	*CI-1	(1,-1,0)(1,1,0)(1,0,1)	(1/2,0,0)
L	1+	3	0	0	4	*CI-1	(2,0,0)(0,2,0)(0,0,1)	(0,0,0)
L	1+	3	0	0	4	CI-1	(2,0,0)(0,2,0)(0,0,1)	(0,0,0)
L	1+	3	0	0	8	*C3I-2	(2,0,0)(0,2,0)(0,0,1)	(0,0,0)
L	1+	3	0	0	8	CI-1	(2,0,0)(0,2,0)(0,0,2)	(0,0,0)
L	1-	3	0	0	2	*CI-1	(1,0,0)(0,2,0)(0,0,1)	(0,1/2,0)
L	1-	3	0	0	4	CI-1	(2,0,0)(0,2,0)(0,0,1)	(1/2,1/2,0)
L	1-	3	0	0	8	*C3I-2	(2,0,0)(0,2,0)(0,0,2)	(1/2,1/2,1/2)
L	1-	3	0	0	8	CI-1	(2,0,0)(0,2,0)(0,0,2)	(1/2,1/2,1/2)
F	1+	3	1	0	2	CI-1	(1,0,0)(0,0,-1)(0,1,1)	(0,0,0)
F	1+	3	1	0	4	C3I-2	(-1,1,1)(1,-1,1)(1,1,-1)	(0,0,0)
F	1+	3	1	0	4	CI-1	(1,-1,-1)(1,1,-1)(1,1,1)	(0,0,0)
F	1-	3	0	0	2	*CI-1	(1,0,0)(0,1,-1)(0,1,1)	(0,1/2,0)
F	1-	3	0	0	4	*C3-4	(-1,1,1)(1,-1,1)(1,1,-1)	(0,0,0)
F	1-	3	0	0	4	CI-1	(1,-1,-1)(1,1,-1)(1,1,1)	(1/2,1/2,0)
F	1-	3	0	0	4	CI-1	(1,-1,-1)(1,1,-1)(1,1,1)	(0,0,0)

TABLE V

$$T(\Gamma,E) = \begin{pmatrix} E & 0 & 0 & 0 & 0 & 0 \\ 0 & E & 0 & 0 & 0 & 0 \\ 0 & 0 & E & 0 & 0 & 0 \\ 0 & 0 & 0 & E & 0 & 0 \\ 0 & 0 & 0 & 0 & E & 0 \\ 0 & 0 & 0 & 0 & 0 & E \end{pmatrix}$$

$$T(\Gamma,I) = \begin{pmatrix} 0 & 0 & 0 & I & 0 & 0 \\ 0 & 0 & 0 & 0 & I & 0 \\ 0 & 0 & 0 & 0 & 0 & I \\ I & 0 & 0 & 0 & 0 & 0 \\ 0 & I & 0 & 0 & 0 & 0 \\ 0 & 0 & I & 0 & 0 & 0 \end{pmatrix}$$

$$T(\Gamma,C_3^+) = \begin{pmatrix} 0 & C_3^+ & 0 & 0 & 0 & 0 \\ 0 & 0 & C_3^+ & 0 & 0 & 0 \\ C_3^+ & 0 & 0 & 0 & 0 & 0 \\ 0 & 0 & 0 & 0 & C_3^+ & 0 \\ 0 & 0 & 0 & 0 & 0 & C_3^+ \\ 0 & 0 & 0 & 0 & C_3^+ & 0 \end{pmatrix}$$

$$T(\Gamma, C_3^-) = \begin{pmatrix} 0 & 0 & C_3^- & 0 & 0 & 0 \\ C_3^- & 0 & 0 & 0 & 0 & 0 \\ 0 & C_3^- & 0 & 0 & 0 & 0 \\ 0 & 0 & 0 & 0 & 0 & C_3^- \\ 0 & 0 & 0 & C_3^- & 0 & 0 \\ 0 & 0 & 0 & 0 & C_3^- & 0 \end{pmatrix}$$

$$T(\Gamma, S_6^+) = \begin{pmatrix} 0 & 0 & 0 & 0 & 0 & S_6^+ \\ 0 & 0 & 0 & S_6^+ & 0 & 0 \\ 0 & 0 & 0 & 0 & S_6^+ & 0 \\ 0 & 0 & S_6^+ & 0 & 0 & 0 \\ S_6^+ & 0 & 0 & 0 & 0 & 0 \\ 0 & S_6^+ & 0 & 0 & 0 & 0 \end{pmatrix}$$

$$T(\Gamma, S_6^-) = \begin{pmatrix} 0 & 0 & 0 & 0 & S_6^- & 0 \\ 0 & 0 & 0 & 0 & 0 & S_6^- \\ 0 & 0 & 0 & S_6^- & 0 & 0 \\ 0 & S_6^- & 0 & 0 & 0 & 0 \\ 0 & 0 & S_6^- & 0 & 0 & 0 \\ S_6^- & 0 & 0 & 0 & 0 & 0 \end{pmatrix}$$

TABLE VIa. Γ point small rep characters.

G^{Γ}	E	I	C_3^+	C_3^-	S_6^+	S_6^-
Γ_1^+	1	1	1	1	1	1
Γ_1^-	1	-1	1	1	-1	-1
$\Gamma_2^+ + \Gamma_3^+$	$\begin{pmatrix} 1 & 0 \\ 0 & 1 \end{pmatrix}$	$\begin{pmatrix} 1 & 0 \\ 0 & 1 \end{pmatrix}$	$\begin{pmatrix} -1/2 & -\gamma \\ \gamma & -1/2 \end{pmatrix}$	$\begin{pmatrix} -1/2 & \gamma \\ -\gamma & -1/2 \end{pmatrix}$	$\begin{pmatrix} -1/2 & \gamma \\ -\gamma & -1/2 \end{pmatrix}$	$\begin{pmatrix} -1/2 & -\gamma \\ \gamma & -1/2 \end{pmatrix}$
$\Gamma_2^- + \Gamma_3^-$	$\begin{pmatrix} 1 & 0 \\ 0 & 1 \end{pmatrix}$	$\begin{pmatrix} -1 & 0 \\ 0 & -1 \end{pmatrix}$	$\begin{pmatrix} -1/2 & -\gamma \\ \gamma & -1/2 \end{pmatrix}$	$\begin{pmatrix} -1/2 & \gamma \\ -\gamma & -1/2 \end{pmatrix}$	$\begin{pmatrix} 1/2 & -\gamma \\ \gamma & 1/2 \end{pmatrix}$	$\begin{pmatrix} 1/2 & \gamma \\ -\gamma & 1/2 \end{pmatrix}$

TABLE VI b

G^F	E	I
F_1^+	1	1
F_1^-	1	-1

TABLE VII

$$P_{11}^{3} = \begin{pmatrix} P & -P \\ -P & P \end{pmatrix}$$

with

$$P = \begin{pmatrix}
1 & 0 & 0 & \frac{1}{4} & \frac{\gamma}{2} & 0 & \frac{1}{4} & \frac{-\gamma}{2} & 0 \\
0 & 1 & 0 & \frac{-\gamma}{2} & \frac{1}{4} & 0 & \frac{\gamma}{2} & \frac{1}{4} & 0 \\
0 & 0 & 1 & 0 & 0 & \frac{-1}{2} & 0 & 0 & \frac{-1}{2} \\
\frac{1}{4} & \frac{-\gamma}{2} & 0 & 1 & 0 & 0 & \frac{1}{4} & \frac{\gamma}{2} & 0 \\
\frac{\gamma}{2} & \frac{1}{4} & 0 & 0 & 1 & 0 & \frac{-\gamma}{2} & \frac{1}{4} & 0 \\
0 & 0 & \frac{-1}{2} & 0 & 0 & 1 & 0 & 0 & \frac{-1}{2} \\
\frac{1}{4} & \frac{\gamma}{2} & 0 & \frac{1}{4} & \frac{-\gamma}{2} & 0 & 1 & 0 & 0 \\
\frac{-\gamma}{2} & \frac{1}{4} & 0 & \frac{\gamma}{2} & \frac{1}{4} & 0 & 0 & 1 & 0 \\
0 & 0 & \frac{-1}{2} & 0 & 0 & \frac{-1}{2} & 0 & 0 & 1
\end{pmatrix}$$

$$P_{21}^{3} = \begin{pmatrix} Q & Q \\ -Q & Q \end{pmatrix}$$

with

$$Q = \begin{pmatrix} 0 & 0 & 0 & \frac{-\gamma}{2} & \frac{-3}{4} & 0 & \frac{\gamma}{2} & \frac{-3}{4} & 0 \\ 0 & 0 & 0 & \frac{3}{4} & \frac{-\gamma}{2} & 0 & \frac{3}{4} & \frac{\gamma}{2} & 0 \\ 0 & 0 & 0 & 0 & 0 & \gamma & 0 & 0 & -\gamma \\ \frac{\gamma}{2} & \frac{-3}{4} & 0 & 0 & 0 & 0 & \frac{-\gamma}{2} & \frac{-3}{4} & 0 \\ \frac{3}{4} & \frac{\gamma}{2} & 0 & 0 & 0 & 0 & \frac{3}{4} & \frac{-\gamma}{2} & 0 \\ 0 & 0 & -\gamma & 0 & 0 & 0 & 0 & 0 & \gamma \\ \frac{-\gamma}{2} & \frac{-3}{4} & 0 & \frac{\gamma}{2} & \frac{-3}{4} & 0 & 0 & 0 & 0 \\ \frac{3}{4} & \frac{-\gamma}{2} & 0 & \frac{3}{4} & \frac{\gamma}{2} & 0 & 0 & 0 & 0 \\ 0 & 0 & \gamma & 0 & 0 & -\gamma & 0 & 0 & 0 \end{pmatrix}$$

FIGURE CAPTIONS

Fig. 1. X-ray peak height and full width at half maximum for the 223 (hexagonal) reflection in $BaMo_6S_8$. The transition temperature (175 K) is indicated by the abrupt drop in peak height and increase in width when the reflection splits in the triclinic phase.

Fig. 2. Raw diffraction data (+) and Rietveld refinement profile (continuous line) for $BaMo_6S_8$ in the $R\bar{3}$ rhombohedral space group at 295 K. Tick marks below the profile mark the positions of all allowed Bragg reflections. A difference plot (observed minus calculated) appears at the bottom. Background has been subtracted prior to plotting.

Fig. 3. Raw diffraction data and Rietveld refinement profile for $BaMo_6S_8$ in the $P\bar{1}$ triclinic space group at 19 K. Format same as Fig. 1.

Fig. 4. Refined peak width parameter versus temperature for $BaMo_6S_8$. This parameter is a measure of the sample-contributed strain broadening and the apparent broadening due to the development of satellites on the shoulders of the $R\bar{3}$ Bragg peaks. Square symbols are for data taken on the first low temperature cycle; round symbols are for later runs.

Fig. 5. Section of the raw diffraction data and best-fit Rietveld profile for a rhombohedral, $R\bar{3}$, refinement model versus temperature. For these plots, the peak width parameter is held at its room temperature value in order to emphasize the departure from $R\bar{3}$ symmetry. The location of the new satellite reflections can most easily be seen in the difference plot at the bottom of each frame.

Fig. 6. Hexagonal a-axis and c-axis lattice constants versus temperature for $BaMo_6S_8$ as determined by Rietveld refinement in $R\bar{3}$ symmetry.

Fig. 7. Unit cell edges (rhombohedral or triclinic) versus temperature for $BaMo_6S_8$. Standard deviations are smaller than the data symbols.

Fig. 8. Unit cell angles (rhombohedral or triclinic) versus temperature for $BaMo_6S_8$. Standard deviations are smaller than the data symbols.

Fig. 9. Unit cell volume (rhombohedral or triclinic) versus temperature for $BaMo_6S_8$. Standard deviations are smaller than the data symbols.

Fig. 10. Bond lengths (Å) in the Mo_6S_8 cluster of $BaMo_6S_8$ at 295 K (a) and 19 K (b). Numbers along the bonds are in units of 0.01Å. The leading digit is 2 for all the bonds shown and has been omitted (e.g., "58" means 2.58 Å). Small circles are Mo atoms; large circles are S atoms. Atom labels follow the convention of the $P\bar{1}$ triclinic structure as in Table II with primed atoms being related to unprimed atoms by inversion through the origin. The [111] axis (rhombohedral or triclinic) is into the paper.

Fig. 11. Mean squared displacement versus temperature for the Ba ion in $BaMo_6S_8$ in the plane perpendicular to the [111] rhombohedral or triclinic axis.

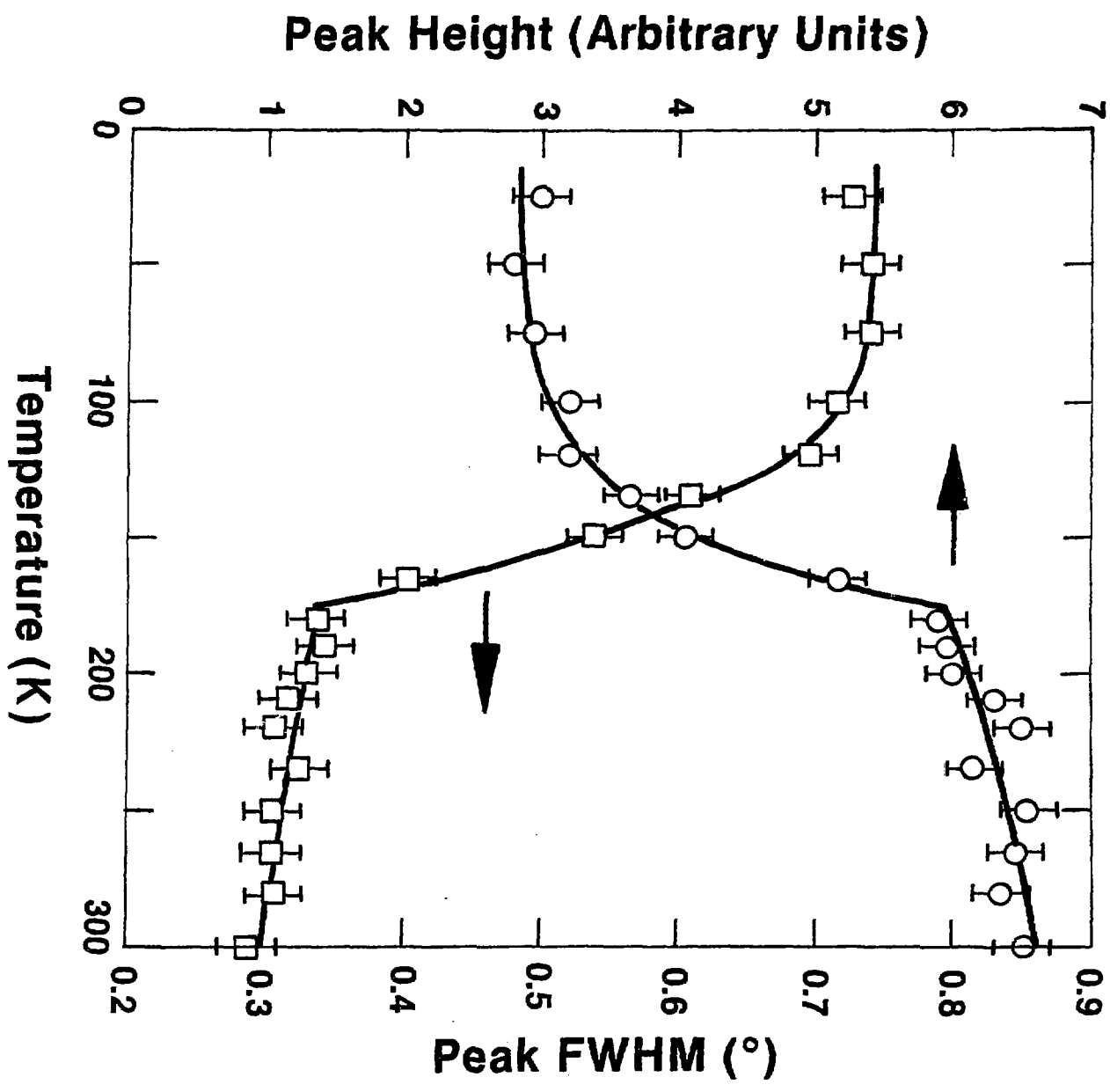
Peak Height (Arbitrary Units)
0
1
2
3
4
5
6
7
Temperature (K)
0
100
200
300
Peak FWHM (°)
0.2
0.3
0.4
0.5
0.6
0.7
0.8
0.9

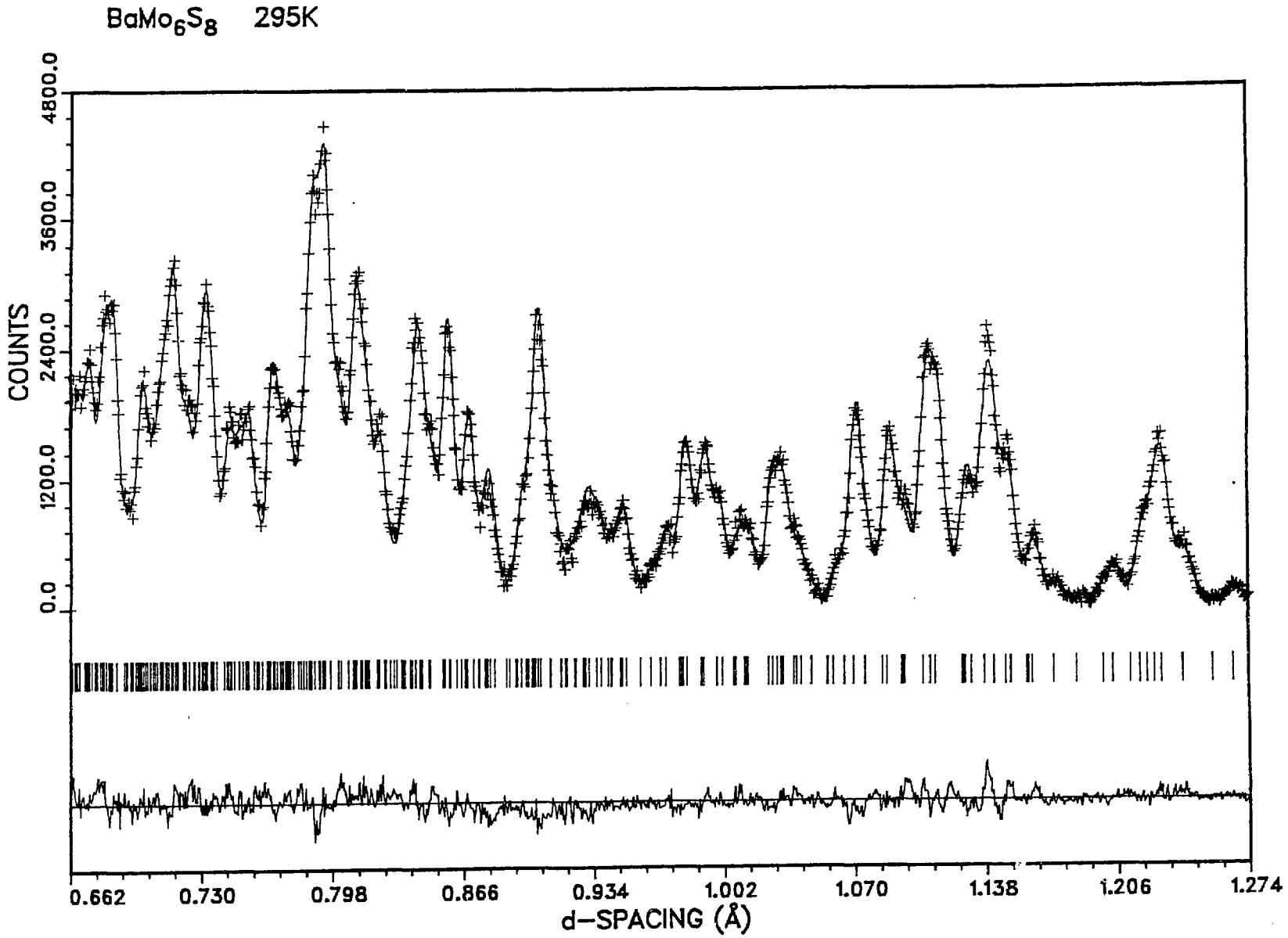
BaMo6S8 295K
COUNTS
4800.0
3600.0
2400.0
1200.0
0.0
0.662
0.730
0.798
0.866
0.934
1.002
1.070
1.138
1.206
1.274
d-SPACING (Å)

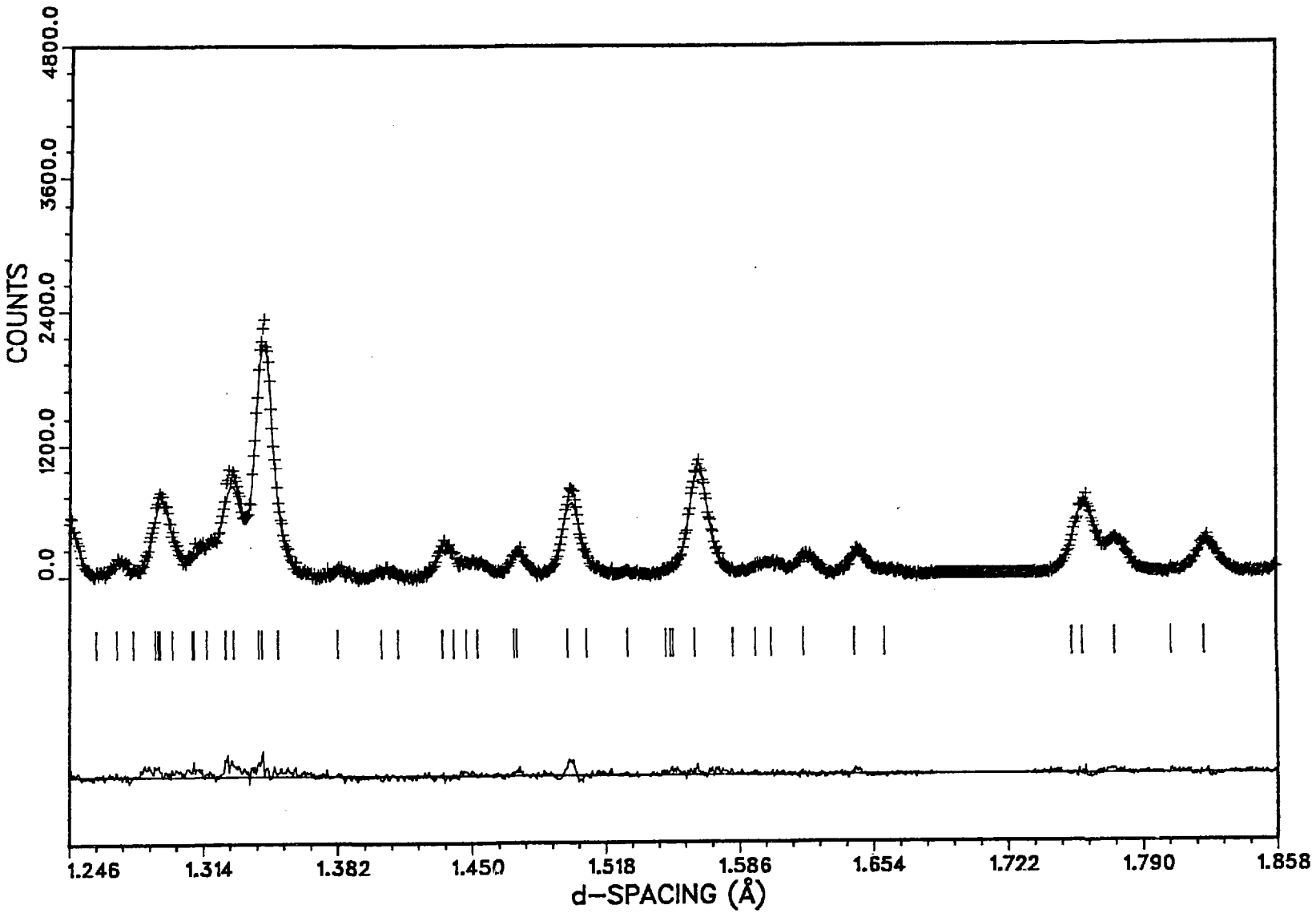
BaMo6S8 295K
COUNTS
4800.0
3600.0
2400.0
1200.0
0.0
1.246
1.314
1.382
1.450
1.518
1.586
1.654
1.722
1.790
1.858
d-SPACING (Å)

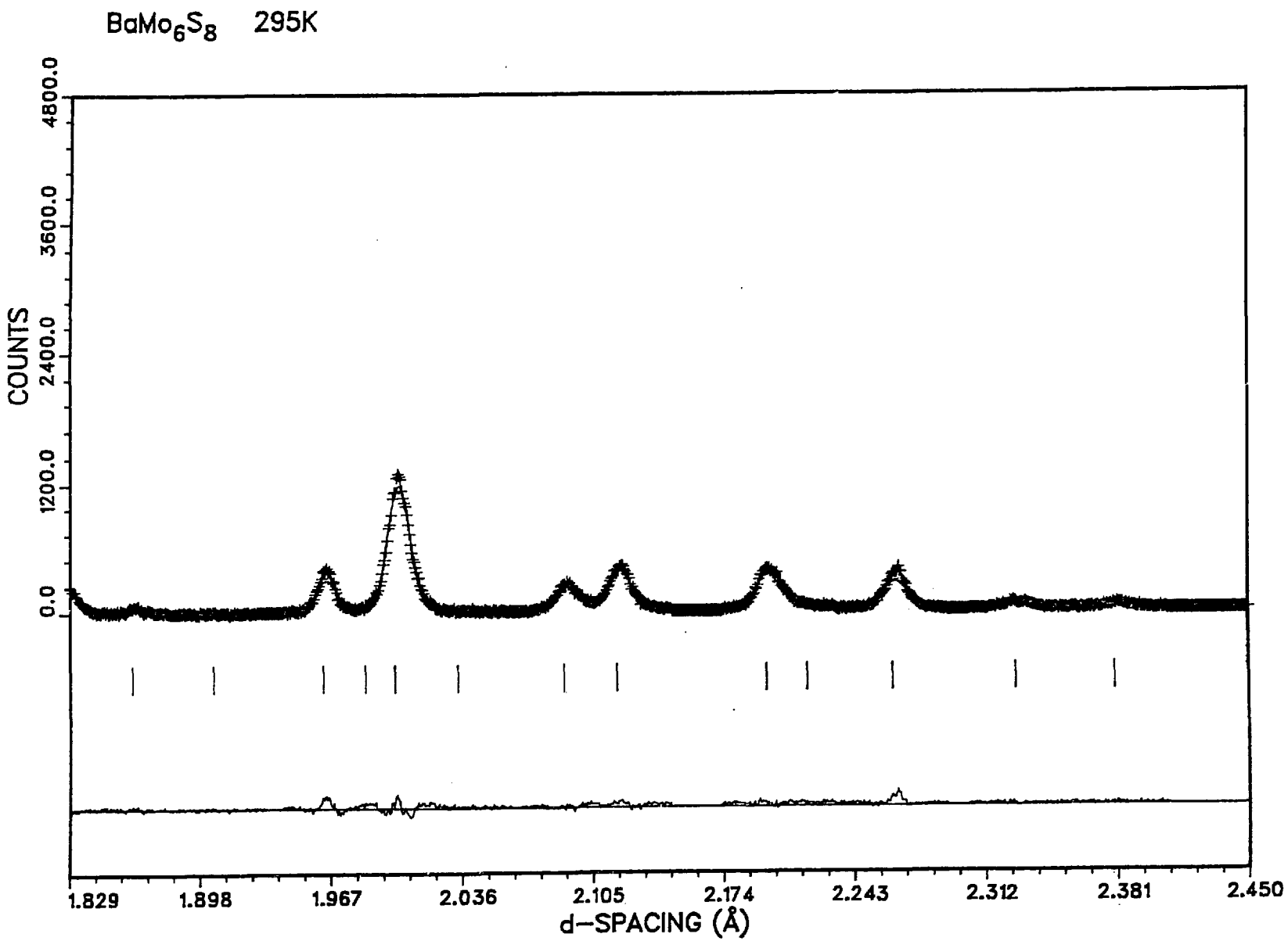
BaMo6S8 295K
COUNTS
4800.0
3600.0
2400.0
1200.0
0.0
1.829
1.898
1.967
2.036
2.105
2.174
2.243
2.312
2.381
2.450
d–SPACING (Å)

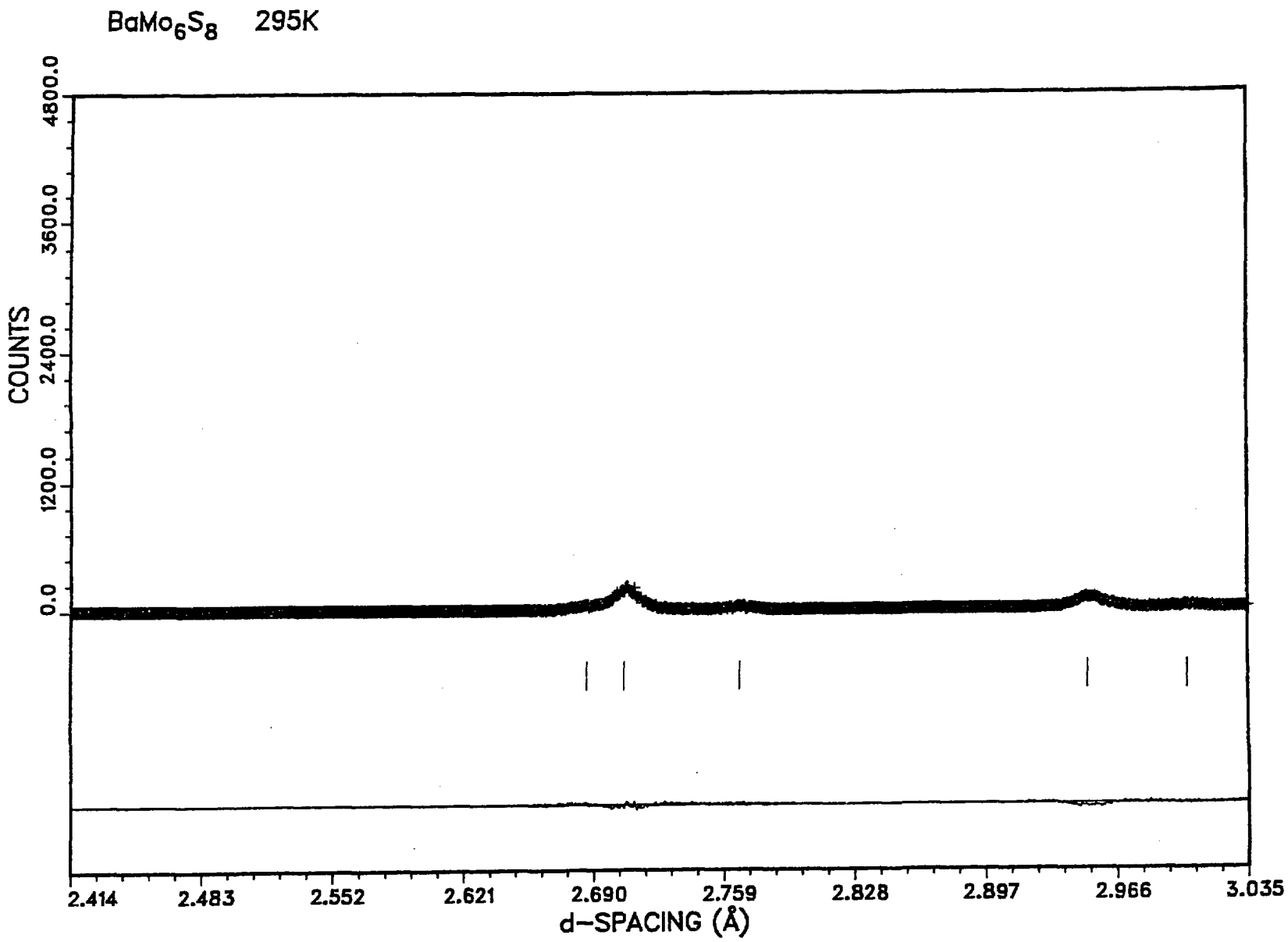
BaMo6S8 295K
COUNTS
4800.0
3600.0
2400.0
1200.0
0.0
2.414
2.483
2.552
2.621
2.690
2.759
2.828
2.897
2.966
3.035
d-SPACING (Å)

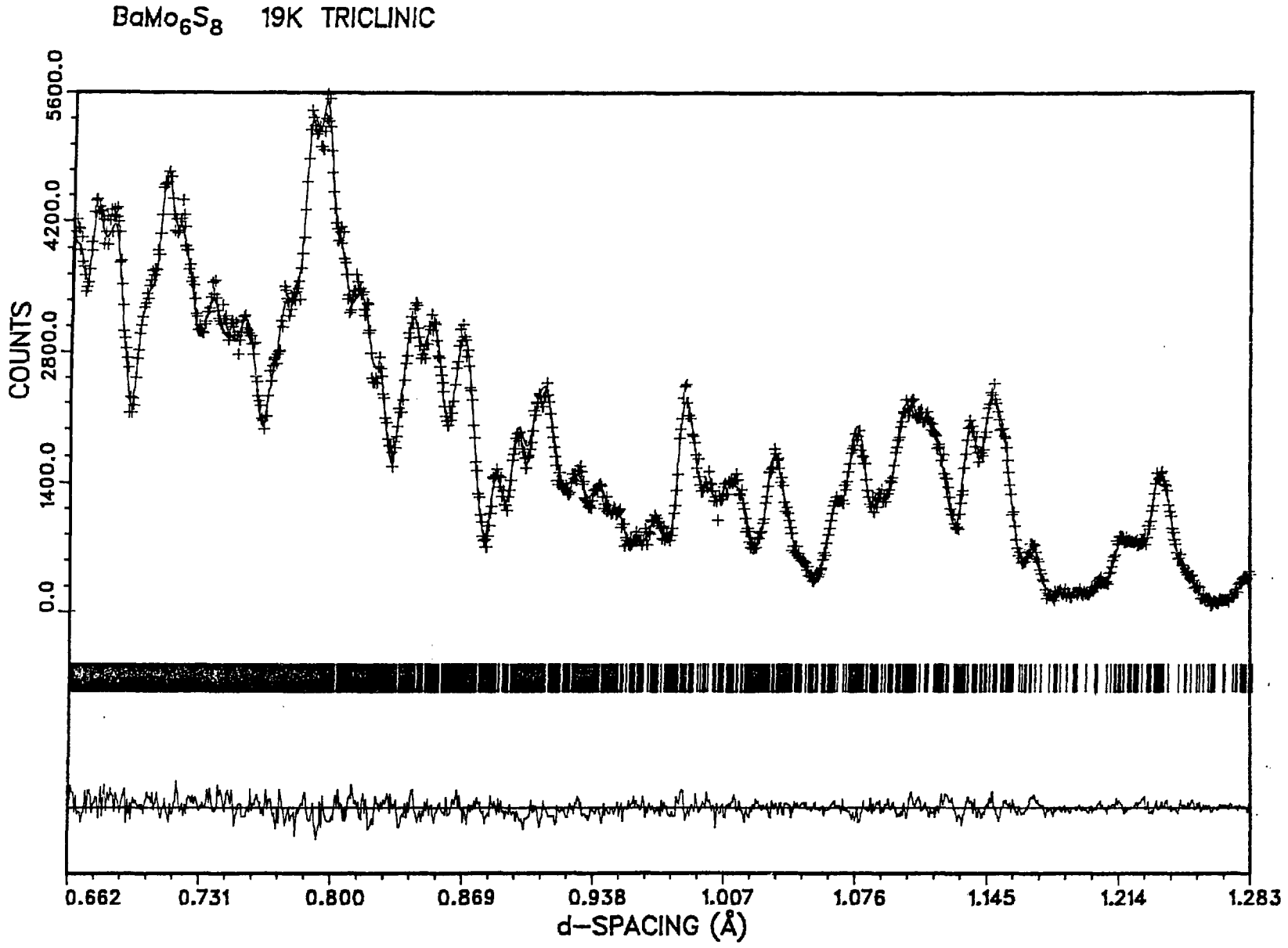
BaMo6S8 19K TRICLINIC
COUNTS
5600.0
4200.0
2800.0
1400.0
0.0
0.662
0.731
0.800
0.869
0.938
1.007
1.076
1.145
1.214
1.283
d–SPACING (Å)

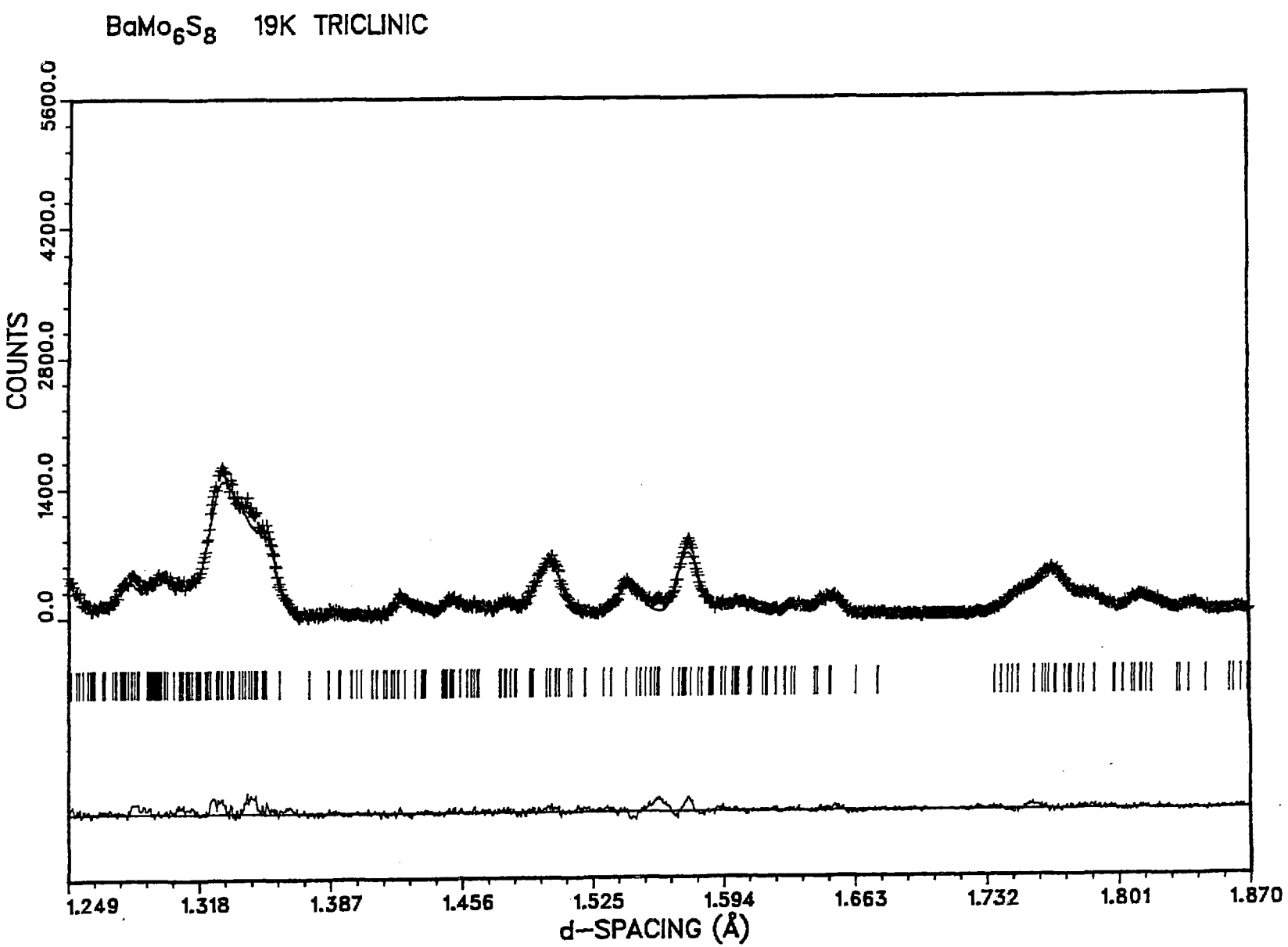
BaMo6S8 19K TRICLINIC
COUNTS
5600.0
4200.0
2800.0
1400.0
0.0
1.249
1.318
1.387
1.456
1.525
1.594
1.663
1.732
1.801
1.870
d-SPACING (Å)

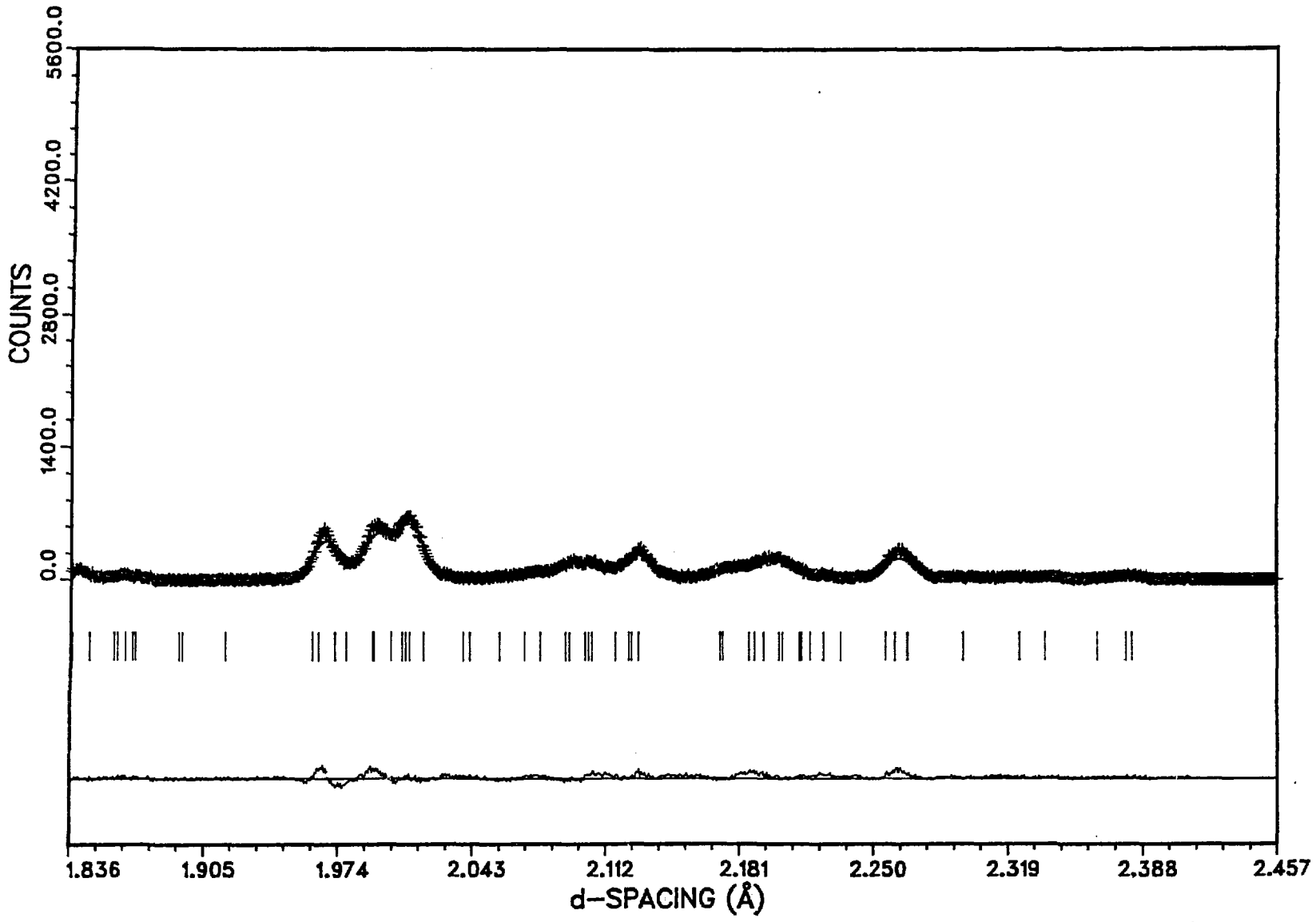
BaMo6S8 19K TRICLINIC
COUNTS
5600.0
4200.0
2800.0
1400.0
0.0
1.836
1.905
1.974
2.043
2.112
2.181
2.250
2.319
2.388
2.457
d-SPACING (Å)

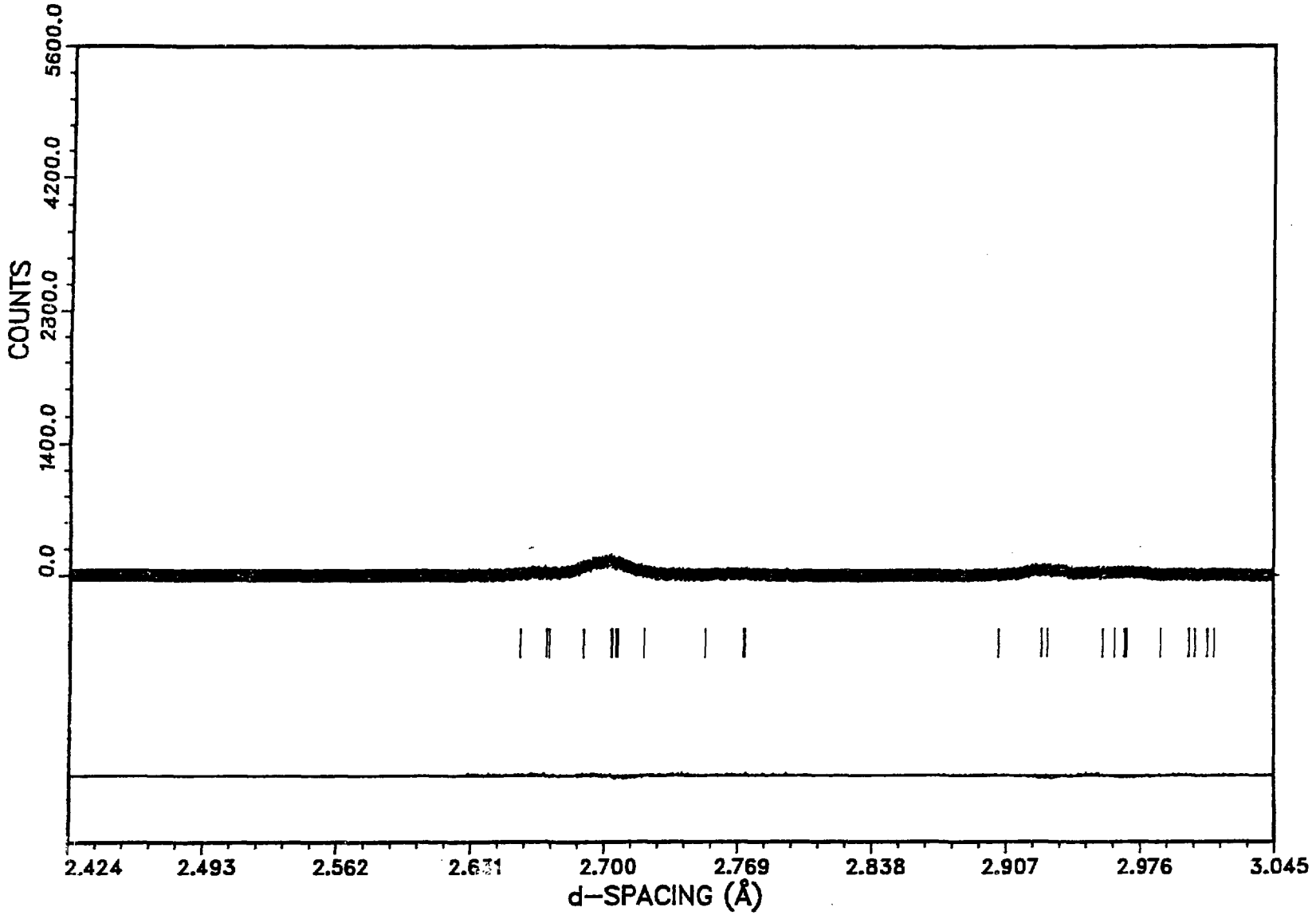
BaMo6S8 19K TRICLINIC
COUNTS
5600.0
4200.0
2300.0
1400.0
0.0
2.424
2.493
2.562
2.631
2.700
2.769
2.838
2.907
2.976
3.045
d–SPACING (Å)

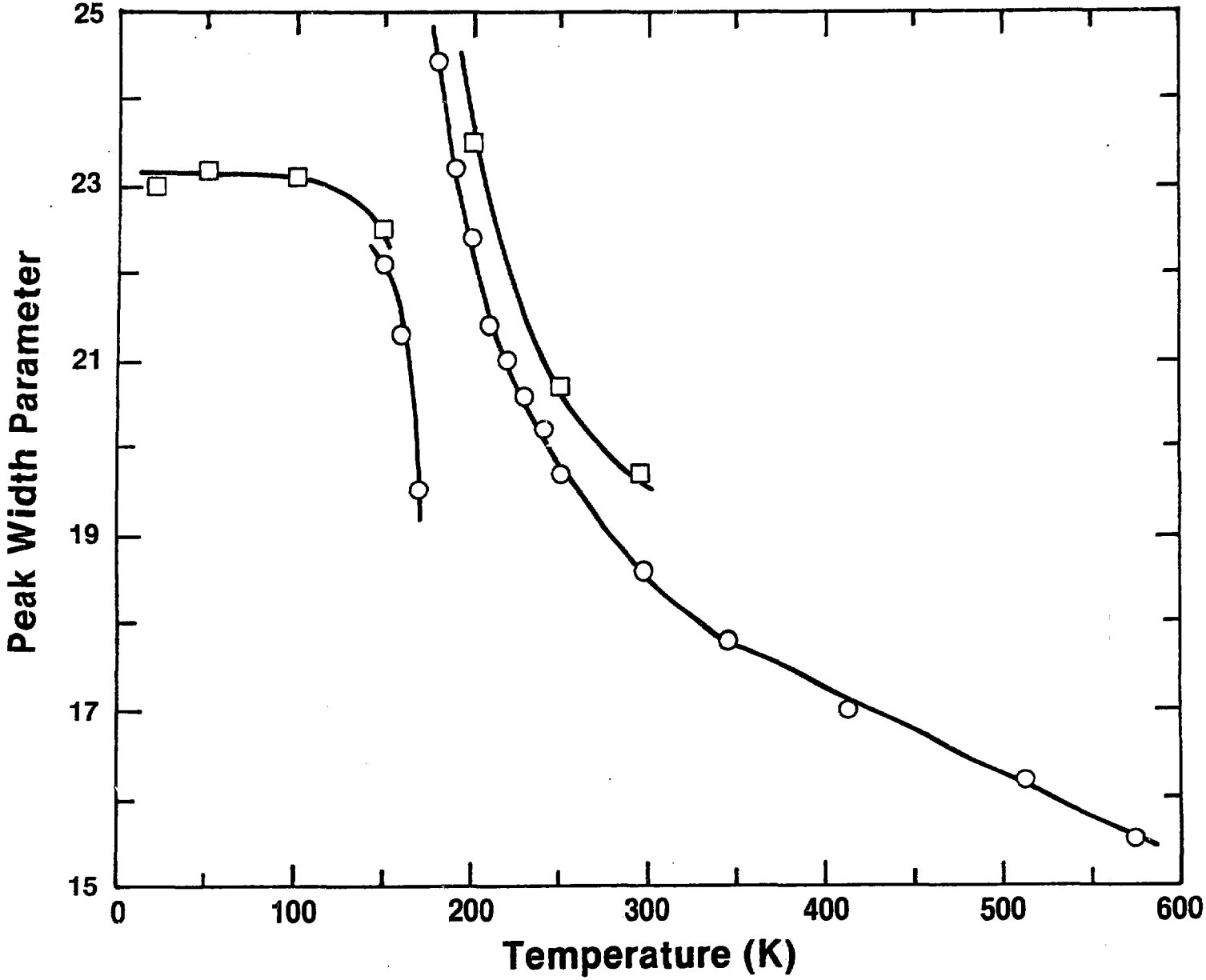
Peak Width Parameter
25
23
21
19
17
15
0
100
200
300
400
500
600
Temperature (K)

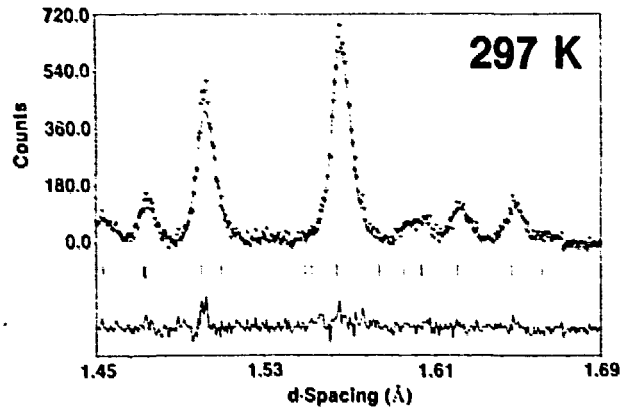
297 K
Counts
720.0
540.0
360.0
180.0
0.0
1.45
1.53
1.61
1.69
d-Spacing (Å)

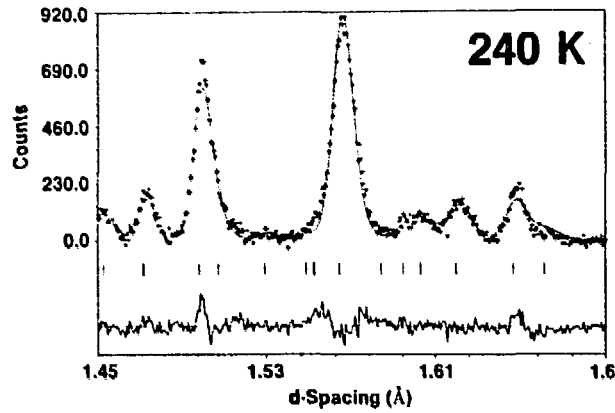
240 K
Counts
920.0
690.0
460.0
230.0
0.0
1.45
1.53
1.61
1.69
d-Spacing (Å)

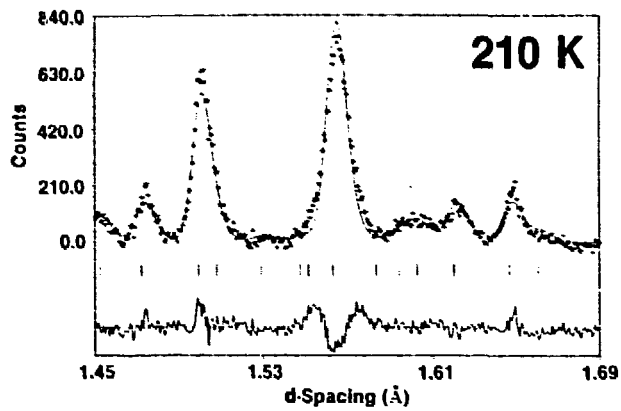
210 K
Counts
840.0
630.0
420.0
210.0
0.0
1.45
1.53
1.61
1.69
d-Spacing (Å)

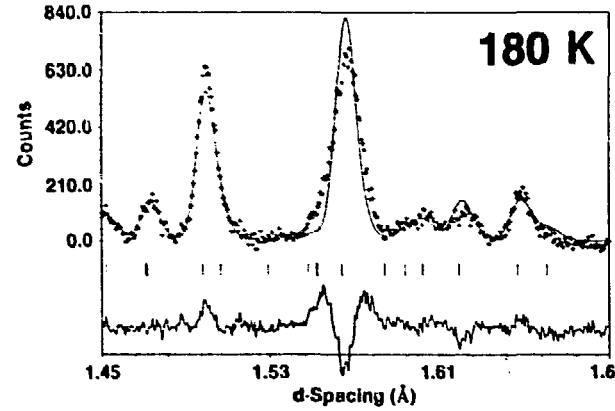
180 K
Counts
840.0
630.0
420.0
210.0
0.0
1.45
1.53
1.61
1.69
d-Spacing (Å)

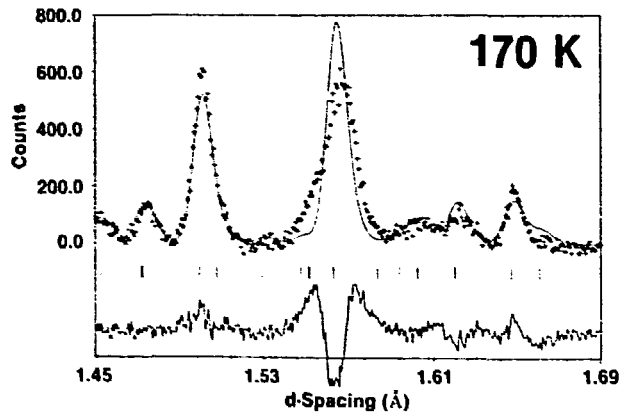
170 K
Counts
800.0
600.0
400.0
200.0
0.0
1.45
1.53
1.61
1.69
d-Spacing (Å)

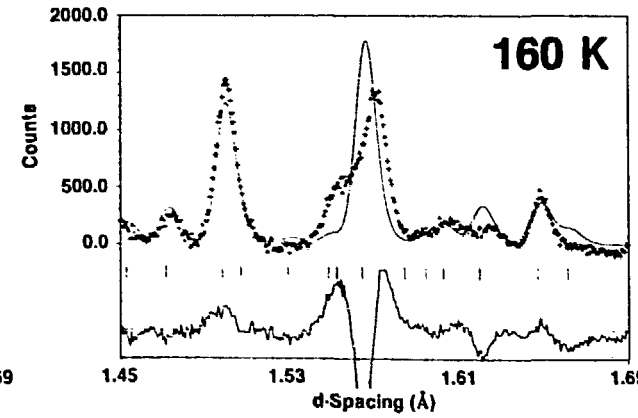
160 K
Counts
2000.0
1500.0
1000.0
500.0
0.0
1.45
1.53
1.61
1.69
d-Spacing (Å)

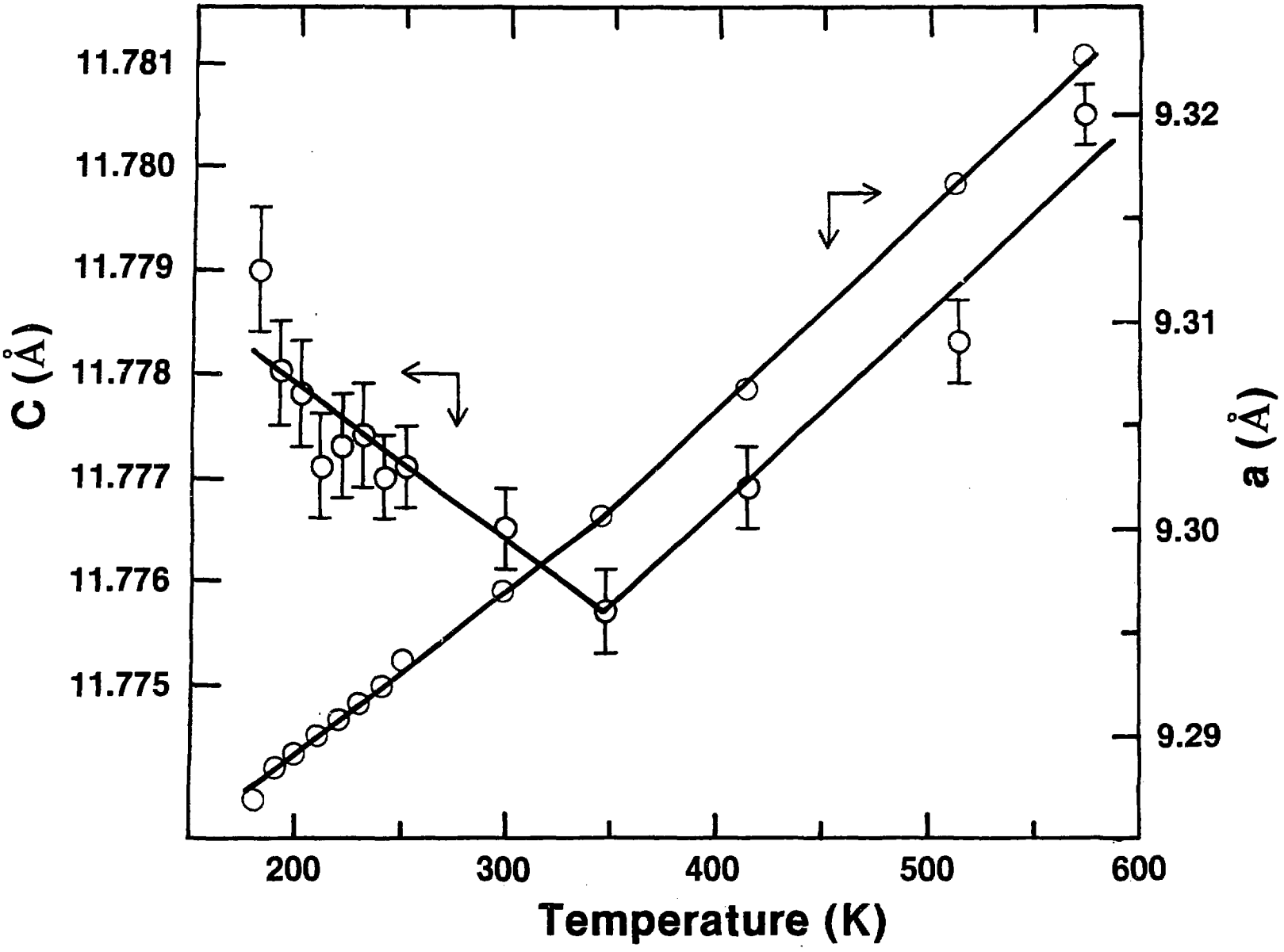
11.781
11.780
11.779
11.778
11.777
11.776
11.775
C (Å)
9.32
9.31
9.30
9.29
a (Å)
200
300
400
500
600
Temperature (K)

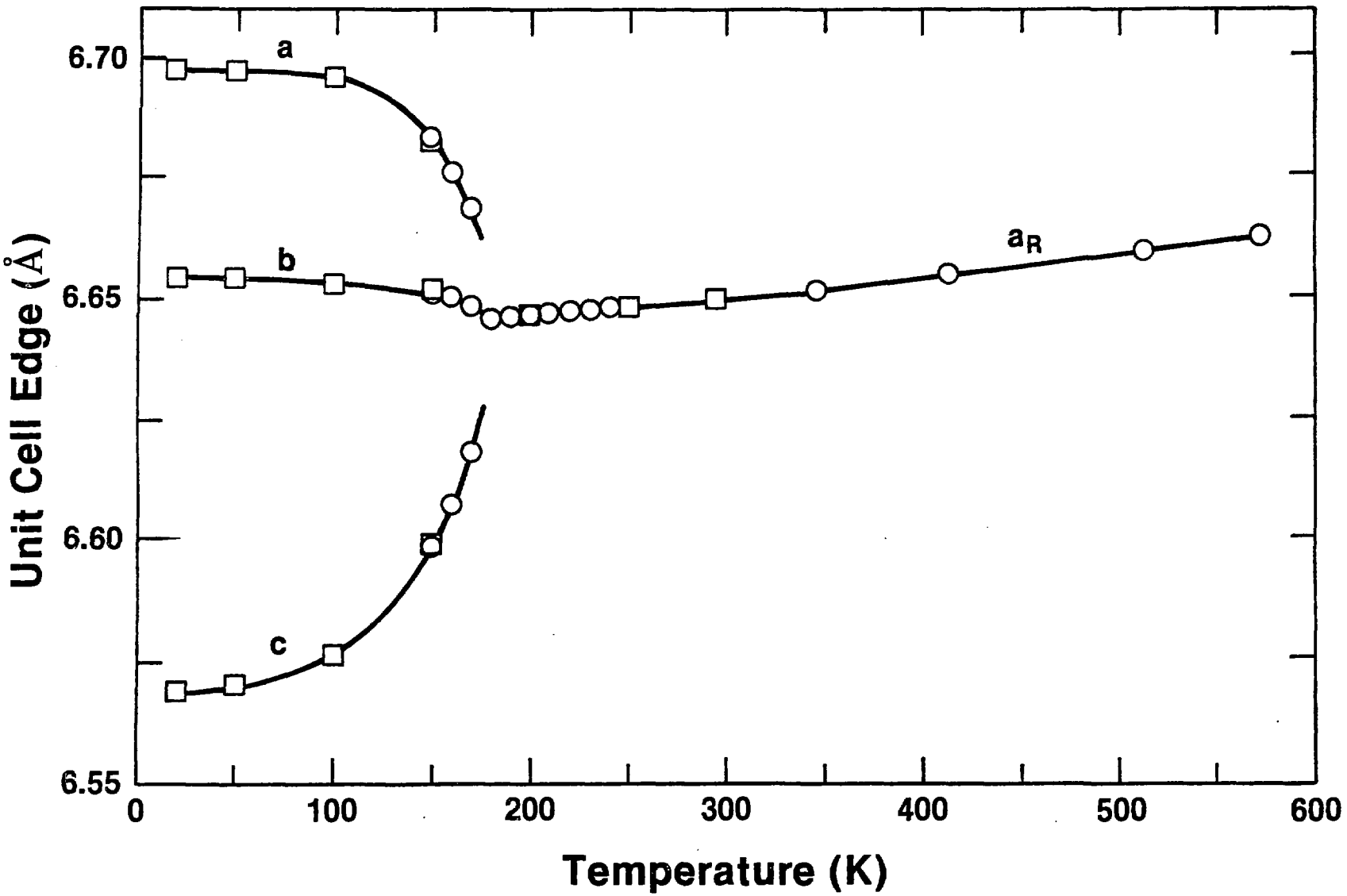
6.70
6.65
6.60
6.55
Unit Cell Edge (Å)
a
b
c
a_R
0
100
200
300
400
500
600
Temperature (K)

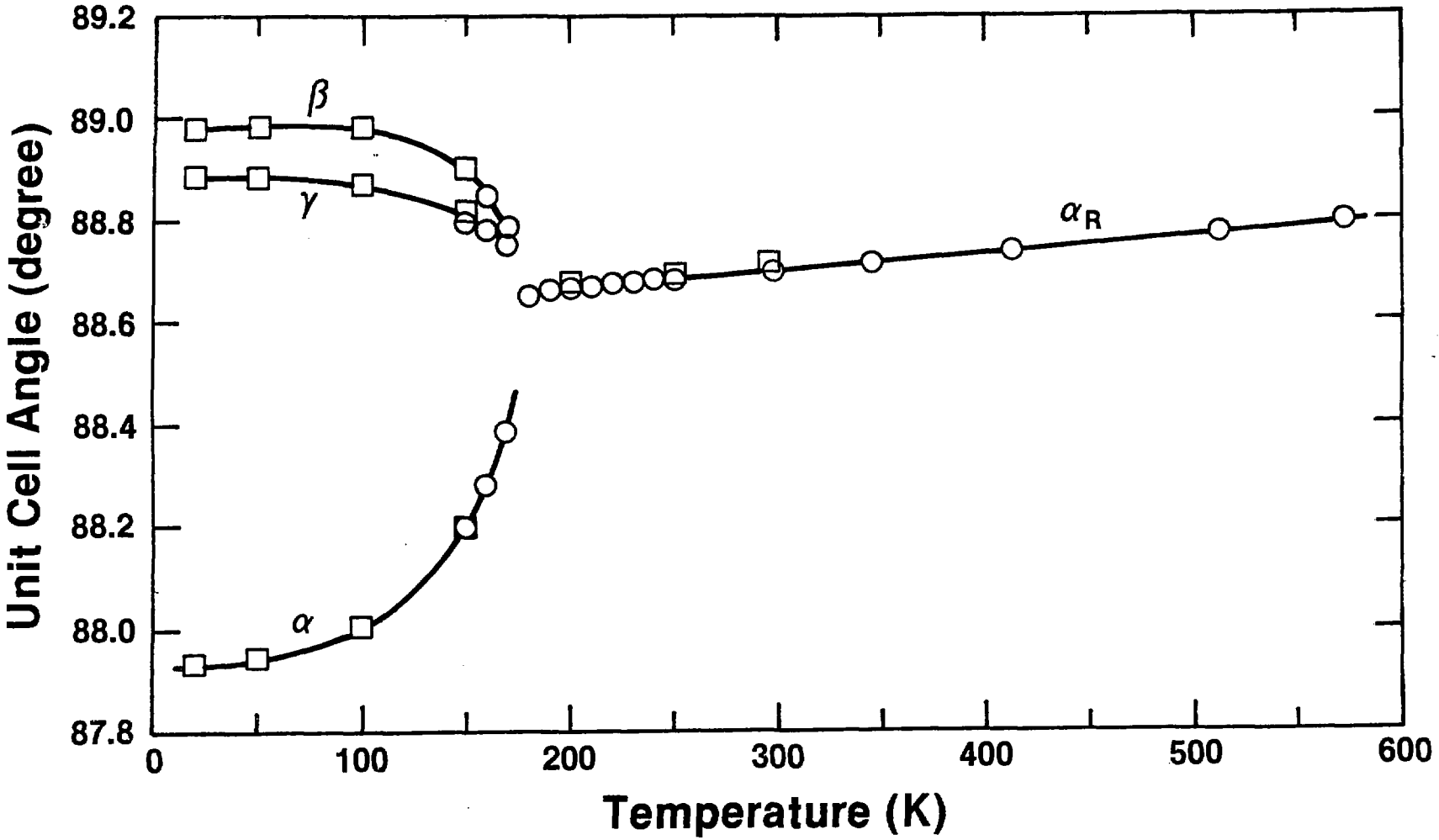
89.2
89.0
88.8
88.6
88.4
88.2
88.0
87.8
Unit Cell Angle (degree)
β
γ
α
α_R
0
100
200
300
400
500
600
Temperature (K)

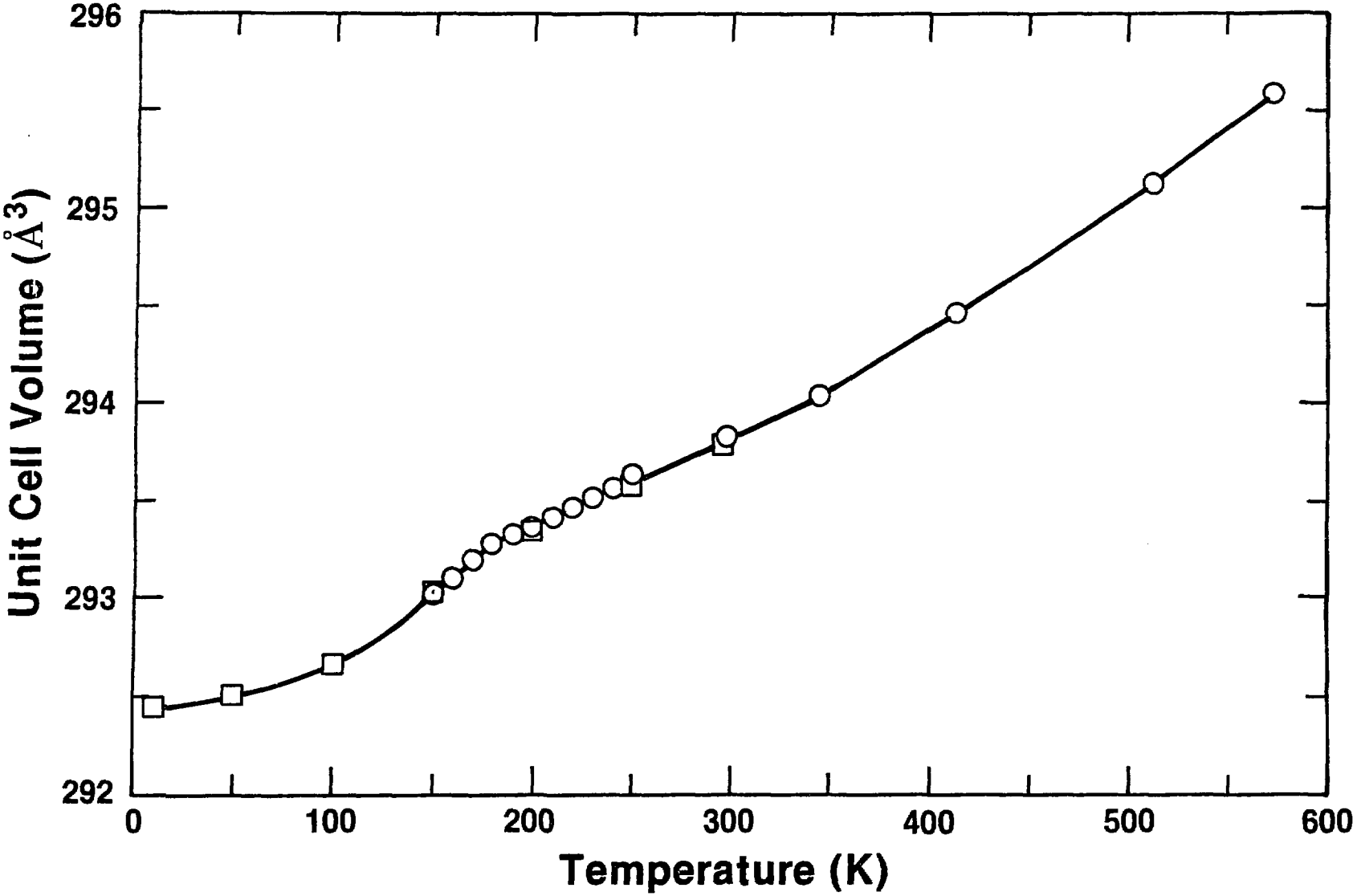
296
295
294
293
292
Unit Cell Volume (Å3)
0
100
200
300
400
500
600
Temperature (K)

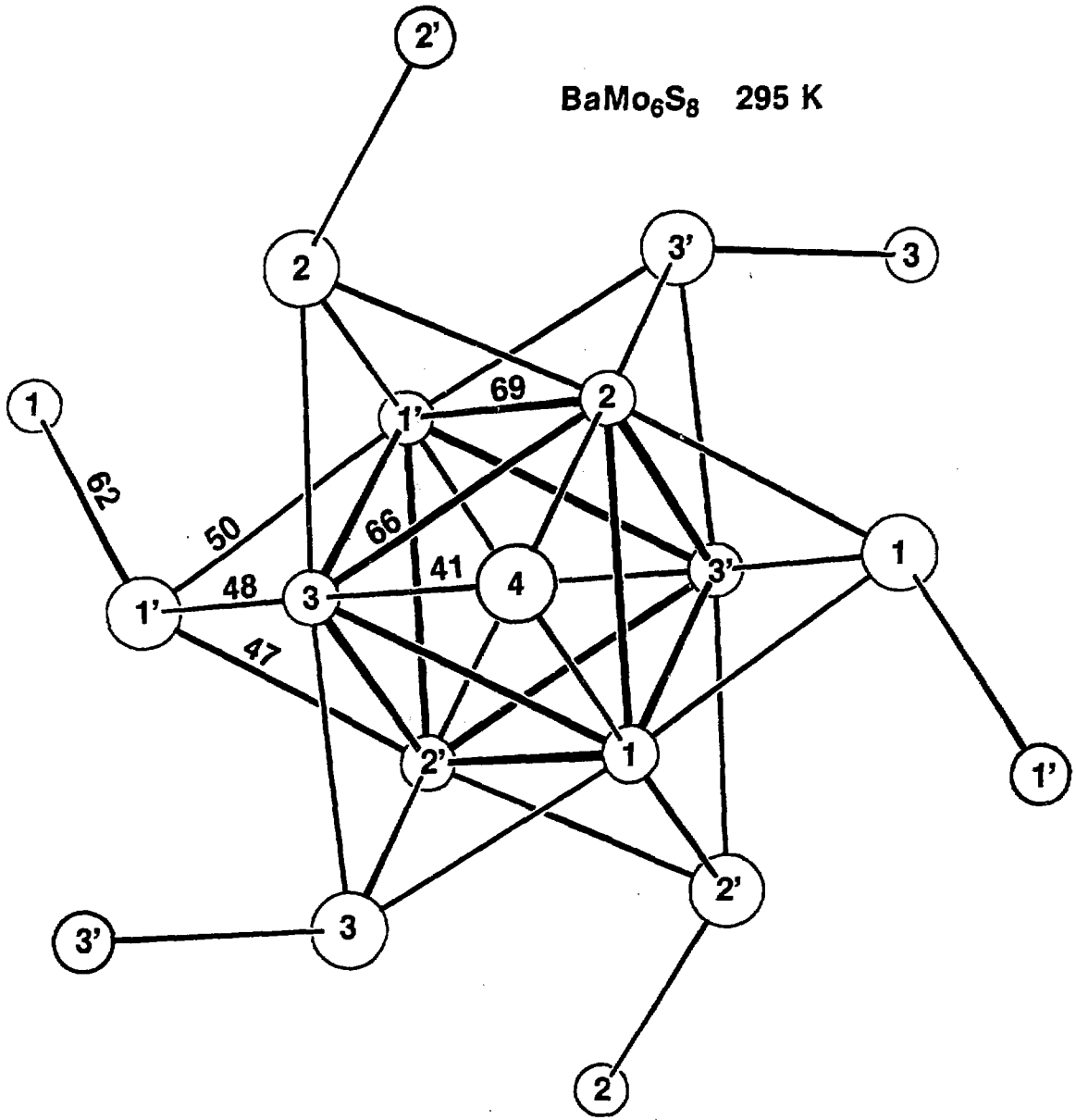
BaMo6S8 295 K
2'
2
3'
3
1
1'
2
69
62
50
66
41
48
4
3'
1
1'
3
47
2'
1
1'
2'
3'
3
2
2

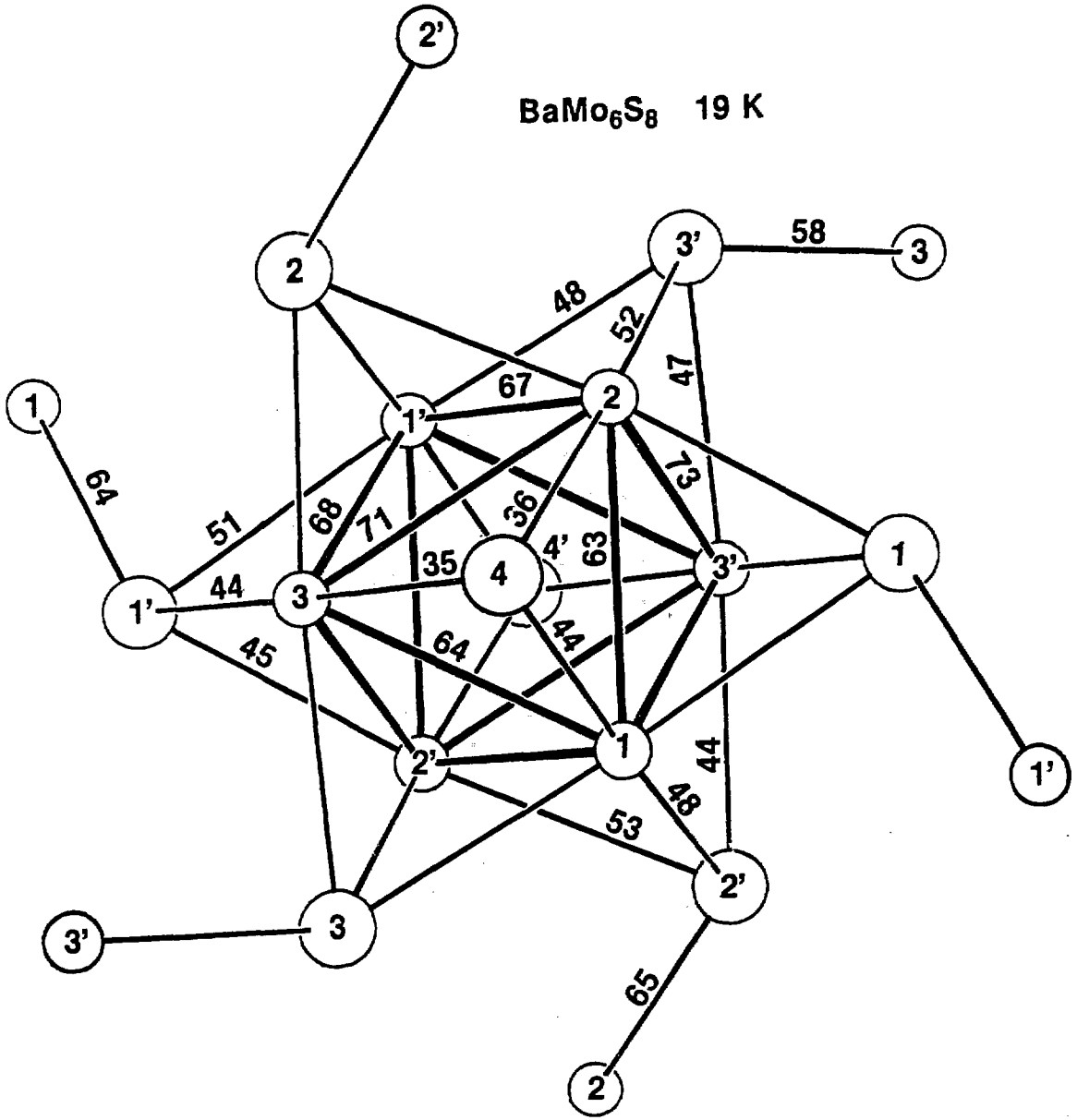
BaMo6S8 19 K
2'
2
3'
58
3
48
52
47
67
1
1'
2
64
51
68
71
36
73
1
4'
63
35
4
3'
1'
44
3
64
44
45
1
1'
2'
44
48
53
2'
3'
3
65
2

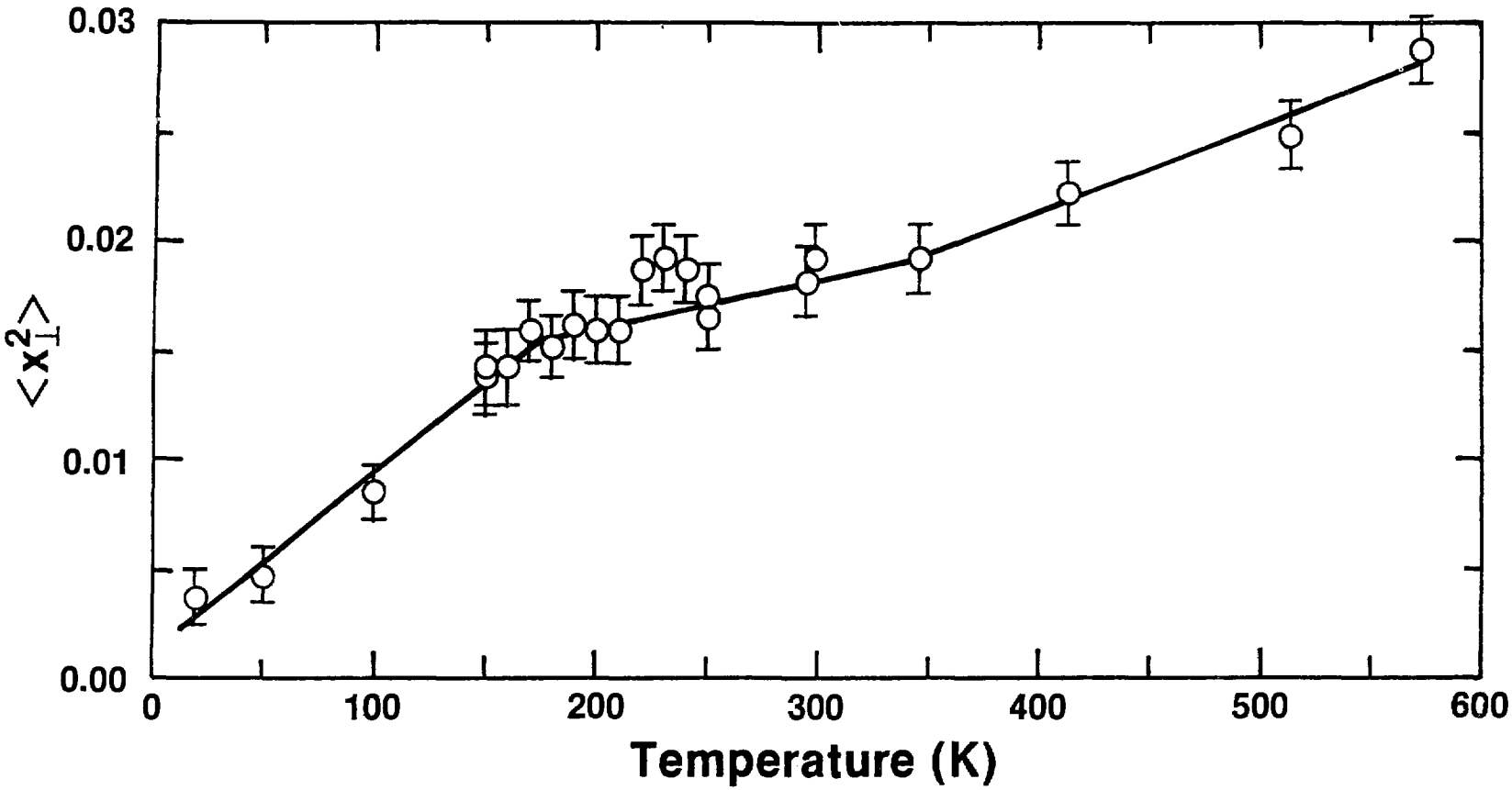
0.03
0.02
0.01
0.00
$\langle x_\perp^2 \rangle$
0
100
200
300
400
500
600
Temperature (K)